Using Synthetic Biology to Investigate And Utilize The Human Skin Microbiome

Alexey Tomsov

Using Synthetic Biology To Investigate And Utilize the Human Skin Microbiome

Research Thesis

In Partial Fulfillment of The Requirements for the Degree of Master of Science in Biotechnology & Food Engineering.

Alexey Tomsov

Submitted to the Senate of the

Technion - Israel Institute of Technology

March 2018 Haifa Adar 5778

The research thesis was done under the supervision of Assist. Prof. Roee Amit in the Department of Biotechnology and Food Engineering.

The generous financial help of the Technion – Israel Institute of Technology (IIT) is gratefully acknowledged.

Table of Content

List of Figures

List of Tables

Abstract

In recent years, the importance of the skin microbiome and its effect on a variety of skin conditions was emphasized in the literature. Skin conditions change the natural skin microbiome; however, the condition-microbiome relationship is not fully understood. Moreover, little is known about the overall stability of genetically engineered members of the skin microbiome that are introduced into the native population. This research aims to use the latest advances in synthetic biology to establish the therapeutic potential of the engineered microbiome.

A set of assays were developed to identify the necessary parameters for stable incorporation of bacteria that are continuously expressing and secreting a heterologous protein, into the native microbiome. The ability to efficiently secrete a heterologous therapeutic enzyme (i.e., 3αHSD) in a bacterial member of the scalp microbiome, *Bacillus subtilis* was demonstrated (US patent application 15/471,194). The hormone that is believed to be the cause of male pattern hair loss, 5α-DHT, is broken down by the 3α-HSD enzyme.

In addition, the viability, heterologous protein expression and dynamic population effects with the natural biota of the engineered strain was investigated using the developed assays. The results indicate that it may be possible to incorporate within the skin microbiome a natural and continuous secretory apparatus that can potentially aid in the continuous delivery of therapeutic agents for a variety of skin conditions.

List of Abbreviations

PBS	Phosphate Buffered Saline
TBS	Tris-Buffered Saline
Hr.	Hour
DNA	Deoxyribonucleic Acid
rRNA	Ribosomal Ribonucleic Acid
Min.	Minute
Cm	Chloramphenicol
Kan	Kanamycin
NGS	Next Generation Sequencing
°C	Celsius Degree
µl	Microliter
µM	Micromolar
g	Standard Gravity
kDa	Kilo-Dalton
PCR	Polymerase Chain Reaction
His	Histidine
mM	Millimolar
mg	Milligram
ng	Nanogram
bp	Base Pairs

List of Abbreviations (Cont.)

nm	Nanometer
OD	Optical Density
rpm	Rounds-per-Minute
V	Volts
v/v	Volume Per Volume
3α-HSD	3α-Hydroxysteroid Dehydrogenase
5α-DHT	5α-Dihydrotestosterone
PHL	Pattern Hair Loss
MPHL	Male Pattern Hair Loss
NADPH	Reduced Nicotinamide Adenine Dinucleotide Phosphate
B. subtilis	*Bacillus Subtilis*
GRAS	Generally Recognized As Safe
Sec Pathway	General Secretory Pathway
TAT Pathway	Twin-Arginine Translocation Pathway
LCST	Lower Critical Solution Temperature
GFP	Green Fluorescent Protein
SP	Signal Peptide
Ori	Origin of Replication
IMT-P8	Institute of Microbial Technology - Peptide 8
LC-MS	Liquid Chromatography - Mass Spectrometry

1 Introduction

1.1 The Importance of The Skin Microbiome Research, Overview

In recent years, the importance of the skin microbiome and its effect on a variety of skin conditions has received increasing attention in the literature. Human skin serves as a primary defense barrier against different pathogens. The skin also contains a vast community of microorganisms that are usually referred to as the skin microbiome. These populations are essential for lipid metabolism and other physiological functions. The skin microbiome differs between areas of the body, different individuals and is affected by environmental factors. Nonetheless, little is known about the overall stability of the skin microbiome, and especially of genetically engineered members of the skin microbiome that are introduced into the native population [1] [2] [3]. Similarly to the gut microbiome, the skin microbiome in healthy adults remains stable for at least two years. This stability was demonstrated for the primary strains included in the skin microbiome populations, as well as for species with relatively low abundance [1].

1.2 Skin Conditions and The Skin Microbiome

Skin conditions temporarily change the natural skin microbiome (e.g., the composition of the microbiome changes throughout inflammation); however, the condition-microbiome relationship, as well as the effect medications and other external conditions might have on the microbiome is poorly understood. Moreover, the skin has distinct physiological properties, with a unique composition of natural substances that may affect different skin conditions (e.g., some unique lipids found on the skin may have antimicrobial activities). The composition of the skin microbiome might be affected by these alterations. Also, the skin microbiome itself might activate immune cells and hence influence a variety of conditions.

To the best of my knowledge, harnessing the microbiome to treat skin conditions has not been adequately demonstrated to date [3] [4].

1.2.1 Male Pattern Hair Loss as A Model for A Possible Engineered Microbiome-Based Solution

As a case study for a skin condition, I chose Male Pattern hair loss (MPHL), also known as Male Pattern Baldness or Androgenic Alopecia. Pattern Hair Loss (PHL) is a form of hair loss, which occurs both in men and women. In men, the gradual hair loss is described by the Hamilton – Norwood baldness scale, with stages starting from a full head of hair, followed by slight frontal recession, followed by vertex hair thinning and eventually a significant hair loss. In women, PHL occurs in the form of hair loss in the central part and described by the Ludwig scale [5]. Men suffer from PHL twice as much as women. Initial signs of MPHL can be observed on average at the age of 14.8 [6]. Moreover, 58% of men will suffer from MPHL by the age of 50, with the percentage increasing up to 73% by the age of 80 [7].
These symptoms, especially when occurring in adolescence, may have psychological and social consequences [5].

It was established in a variety of studies that male pattern baldness is caused by androgens, and especially testosterone and its more potent derivative, 5α-dihydrotestosterone (5α-DHT). Testosterone, the male sex hormone, is being converted by the 5α-reductase enzyme to a more potent derivative, 5α-DHT, on the scalp and other parts of the body [7] [8] [9]. It was demonstrated that the 5α-DHT is an etiologic factor of MPHL, and is believed to be a key cause of this condition [10] [11].
In fact, a significant reduction in the concentration of 5α-DHT on the scalp is correlated to a stop in hair loss and even regrowth of new hair [5].

There are two primary non-surgical solutions approved by the FDA to treat MPHL and available on the market today [5]:

- **Minoxidil**
  A topical, indirect solution that must be applied to the scalp twice daily. The mechanism by which the minoxidil treats MPHL is yet to be described.
  Several suggestions for a mechanism of action were raised, including vasodilation (i.e., increasing the blood flow into the hair follicle), increasing the anagen (active hair follicle growth) phase and simulation of cell proliferation and prostaglandin synthesis. However, it is not yet known how these properties help to treat MPHL [5 12].
  Minoxidil was shown to be effective after application twice a day for 48 weeks. When treatment is terminated, MPHL symptoms return [5].

- **Finasteride**
  An oral drug that contains an azo-steroid that inhibits the action of Type II 5α-reductase. This mechanism reduces the production of 5α-DHT and hence lowers its concentration on the scalp and other parts of the body. In most men treated with finasteride, MPHL is halted [5]. When taken at a 1 $\frac{mg}{day}$ dosage, finasteride shown improvement after 3 months, with even higher significance in the course of 2 years (i.e., stop of hair loss and even return of hair growth) [11]. Some Finasteride side effects include loss of libido, and its therapeutic effect is terminated when the treatment stops [5].

In fact, both approved treatments presented vary in efficacy between different individuals, and when treatment is stopped – the symptoms usually return [5]. As explained in the following sections and chapters, I aim to address some of these limitations with a continuous topical therapeutic delivery (unlike the short-term delivery of minoxidil) of

an agent that breaks down 5α-DHT locally. In this manner, I aim to minimize side effects associated with Finasteride while still targeting the cause of MPHL, 5α-DHT.

1.2.2 3α-HSD As A Therapeutic Agent

5α-DHT can be converted to a less potent derivative called 3α-androstanediol by the 3α-hydroxysteroid dehydrogenase enzyme (3-αHSD). This enzyme utilizes NADPH as a cofactor of the reaction, as can be seen in figure 1.1 [13] [14]. I believe that continuously delivered 3-αHSD might provide an easy to use, topical solution for MPHL.

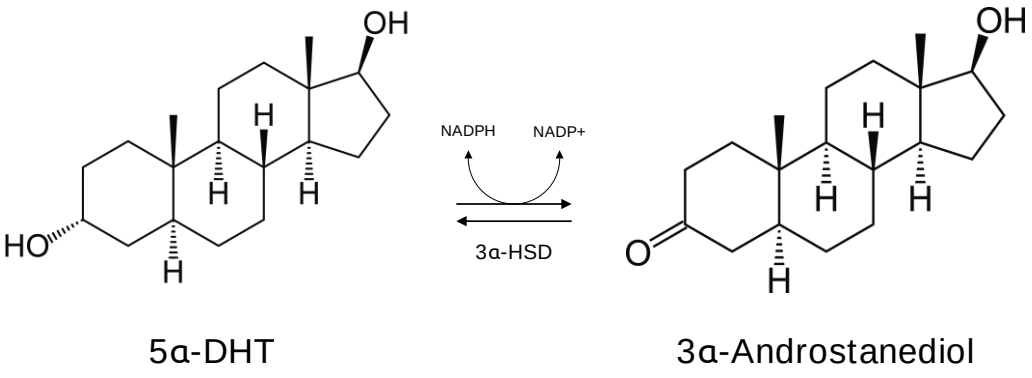

Figure 1.1 *The reaction that is catalyzed by the 3α-HSD (AKR1C14).*

1.3 *Bacillus Subtilis* as a Model for Engineered Microbiome Member Therapeutic Agent Delivery Organism

Bacillus subtilis (*B. subtilis*) is a gram-positive bacteria that was found on the human scalp (i.e., it is part of the natural scalp microbiome) [15]. *B. subtilis* has several advantages that place it as a promising candidate for expression and secretion of heterologous proteins. Namely, it is easily cultured and genetically engineered in the lab, possesses a powerful secretion ability (as explained in the following section), has a GRAS status, doesn't produce toxic

byproducts and has high product yields and powerful secretion capabilities [15] [16].

B. subtilis secretes proteins naturally, mainly by two mechanisms: the general secretory (SEC) pathway or the twin-arginine (TAT) pathway. The signaling for secretion, as well as for the secretion pathway, is done by an N-terminal sequence called a signal peptide (SP), which is recognized by the translocation apparatus. Most secreted proteins are transformed in the unfolded state (conjugated to the SP) through the SEC pathway. The SP is cleaved at the cell membrane by the translocation machinery. Only at the outside of the cell, the secreted proteins are fully folded. In the TAT pathway (which is less characterized compared to the SEC pathway), proteins are usually fully folded within the cell before being translocated to the outside of the cell. It is more challenging to use the TAT pathway for secretion of heterologous proteins [16]. In order to obtain an efficient secretion of an active heterologous protein, it is crucial to tailor a specific SP for every secreted protein. Hence, screening for activity of a secreted heterologous protein that was designed with a library of different SPs conjugated to its gene is recommended [17].

1.3.1 Polymeric Delivery Scaffold

To ensure our engineered population's survival within the larger microbiome, I hypothesized that a growth advantage or protection might be needed. To that end, the engineered microbiome member (*B. subtilis*) was incorporated in a polymeric scaffold that promotes bacterial growth in the natural environment and protects it from local competition in its environmental niche. To formulate such a delivery system, a temperature-responsive polymeric solution was implemented. While stored in the refrigerator the formula will be in liquid form, but upon administered to the scalp, it will solidify to form a stable, transparent gel. In addition, the formula will adhere to the scalp without interfering with the natural regeneration of the bacteria. Temperature-responsive polymers exhibit a drastic and discontinuous change of their physical properties with temperature or

in other words they utilize temperature change as the trigger that determines their gelling behavior without any additional external factor [18]. The polymer that was used is Pluronic® F127 (formulated, tested and generously provided by the Mizrahi lab, Technion) with lower critical solution temperature (LCST) ranging at the 20-36˚C range, below which the formulation is in a water-soluble form. Above the LCST the polymers density increases and a hard and stable gel is formed, a range which is close to the physiological temperature (37˚C) [19].

1.4 Skin Microbiome Research Challenges

In recent years, the importance of microbiome research has been emphasized in the literature. Microbiome research concentrated on several niches in the body, mostly the gut microbiome.
As a result, there is a need for common language and methods for skin microbiome research, due to the skin's unique physiological properties that differentiate it from other bodily niches (e.g., exposure to air, surface pH, low bacterial biomass and contamination risk). As studies of skin microbiome receive increased interest, the field has begun to understand the importance of standardized research methods that are tailored for the skin microbiome [20].
In this work, two standardized experimental assays were developed and specifically designed with the unique niche properties of the skin in mind.

1.4.1 *luxABCDE* As A Marker for Cell Proliferation and Heterologous Protein Production

One of the initial goals was to create an engineered *B. subtilis* (engineered microbiome member) that can be easily detected and differentiated from other skin microbiome members.
Moreover, it was aimed to specifically identify heterologous protein production in this engineered population, with minimal external complexity factors (e.g., external substrate supplementation).

With these goals in mind, I chose to work with the *luxABCDE* bioluminescence construct, a reporter cassette that contains five genes (as can be seen in figure 3.2). I chose to use this cassette over other reporters (e.g., GFP) because of two essential characteristics. First, when expressed in the cell, it emits an entirely autonomous bioluminescent signal, with no need for an exogenous substrate to be supplemented. The bioluminescent reaction involves metabolites naturally found in the cell: $FMNH_2$, O_2, and RCHO (fatty aldehyde). This reaction is shown figure 1.2 and catalyzed by the bacterial luciferase – a heterodimeric enzyme encoded by the *luxA* and *luxB* genes. The bioluminescent light is emitted at λ~480-490 nm (blue-green) [21].

$$FMNH_2 + O_2 + RCHO \rightarrow FMN + H_20 + RCOOH + Light$$

Figure 1.2 *The bioluminescent reaction catalyzed by the heterodimeric enzyme encoded by the luxA and luxB genes [21].*

The other three genes in the *luxABCDE* gene cassette, *luxC*, *luxD*, and *luxE*, encode for three different proteins that take tetradecanoic acid from the fatty acid biosynthesis and form a fatty aldehyde (RCHO) needed for the bioluminescent reaction presented in figure 1.2.
The reactions catalyzed by the *luxC*, *luxD* and *luxE* gene products is presented in figure 1.3. First, *luxD* gene product cleaves tetradecanoyl-ACP (RCO-X). In the following step, the resulting fatty acid (RCOOH) is activated by the *luxE* gene product with ATP. The acyl group from the acyl-AMP created (RCO-AMP) is transferred to *luxE* by the *luxC*, following a reduction step with NADPH [21].

$$\text{RCO-X} \xrightarrow{\text{LuxD}} \text{RCOOH} \xrightarrow{\text{LuxE, ATP}} \text{RCO-AMP} \rightarrow \text{RCO-}\textit{Lux}\text{E} \xrightarrow{\text{LuxC, NADPH}} \text{RCO-}\textit{Lux}\text{C} \rightarrow \text{R-CHO}$$

Figure 1.3 *The reactions catalyzed by the luxC luxD and luxE gene products [21].*

The second reason for choosing the luxABCDE cassette is the fact that unlike GFP which has a long half-life of its signal, luxABCDE emits a real-time signal which reports active transcription of the cassette in the cell [22].

As explained in the following chapters, the cloning of the luxABCDE cassette not only allowed a straightforward identification of the engineered *B. subtilis* (i.e., examine the expression of the heterologous protein in the native environment) but also provided a way to distinguish it from other populations found on the skin.

1.4.2 NGS as A Sequencing Methodology

Two principal methods were described for DNA sequencing and identification of the different communities in the skin microbiome [20]:

- **Shotgun Metagenomic Sequencing**
  Due to the increased sequencing capacities available today, it is more feasible than ever to use this method to sequence skin sample [20]. In this method, the DNA sample is initially broken down to create small random fragments, which are then sequenced. These overlapping sequences are then aligned to create the final sequence [23]. The advantages of this methods are the ability to sequence microorganisms from different kingdoms (i.e., bacteria, fungi and others), and a minimal amplification bias. The disadvantages of this method include complex analysis of the results and a significant sensitivity for contamination by DNA from external sources due to relatively low biomass on the skin [20].

- **Gene Amplicon Sequencing**
  Considered as the most widely used method.
  First, the DNA is extracted from the sample. In the following step, specific DNA fragments are amplified using a dedicated pair of PCR primers. The most used gene in these types of

studies is the 16S rRNA bacterial gene, sequencing one or several of its nine variable regions. V1-V3 are the most used regions to sequence and considered to be the most accurate in classifying skin bacteria. To sequence and identify the fungal community on the skin, other ribosomal regions are targeted, namely the 5.8S, 28S, 18S and internal transcribed spacer. Other parameters of amplification process (e.g., the number of PCR amplification cycles) were considered to reduce the bias associated with this method [20].

To quantify the proliferation of the engineered microbiome member, as well as to identify how the addition of different mediums and bacterial formulations affect the native skin microbiome, I aimed to adopt the most widely used sequencing method – 16S rRNA gene amplicon sequencing, to use for skin microbiome samples [20].

One significant aspect that is mentioned in the literature as a future need is the ability to not only rely on sequencing results but also have additional methods to characterize the skin microbiome.
It is emphasized in the literature that there's a need to have a visualization technique of the skin microbiome. This ability may help to decipher the structure and interrelations of the skin microbiome communities [20]. As a potential answer for this need, I describe in this thesis The Imaging Assay, a complementary part of The NGS Assay and part of the Skin Microbiome Research Toolbox I developed.

Another future need that is emphasized in the literature is the need to have data from several time points that will illustrate the dynamics of the skin microbiome overtime [20]. I answer this need in this thesis as well, both in The NGS assay and The Imaging Assay, as described in the following sections and chapters.

1.4.3 MPHL As A Case Study

The microbiome is a stable microbial population that co-exists with the host [2 4]. While this work discusses a solution for MPHL, it is presented as a proof of principle. Other conditions might also be potentially treated by appending engineered bacteria to the natural microbiome.

In one example from the literature, a strain of the skin microbiome, *Staphylococcus epidermidis,* that produces a substance that inhibits DNA polymerase was isolated from the human skin. This strain might protect the host against skin cancer using the secreted protein. In an *iv-vivo* experiment, colonization of mice with this strain reduced the number of tumors developed compared to mice with a control strain. Although the researchers discussed the potential mutagenic activity of this strain, no in-depth analysis of the effect of such an inoculation on the native microbiome was performed. Moreover, no heterologous protein production approach that might introduce other beneficial anticancer proteins to the skin was discussed [24].

An additional example from the literature described a native protein with antioxidant capacity that is secreted by a skin microbiome member, *Propionibacterium acnes* and hypothesized what effects a knockout of this protein might have on the skin. As part of this analysis, a knocked-out strain was introduced to the skin as part of an Immunohistochemistry assay. The researchers acknowledge that the native secretion of this protein was relatively high, and therefore they did not express it recombinantly [25]. The methodologies used by this group for analysis of secreted proteins can be compared to the ones described in this thesis. Although introducing a knocked-out member back to the native environment, the researchers did not examine the effects this inoculation might have on the native microbiome.

By targeting lab-culturable members of each microbiome population, it is possible to engineer those species to secrete a whole set of health-beneficial proteins continuously. Eventually, these engineered members can be returned to the natural niche (e.g., the skin) for them to proliferate and continuously produce the therapeutic agents.

Since many enzymes are used as therapeutic agents to treat skin conditions, the presented approach with the aid of synthetic biology and recombinant DNA technologies, protein engineering, and polymer encapsulation can offer a continues, “on-site” delivery of the desired therapeutic agents in the appropriate dosage with minimal user-interface or involvement [4]. This concept might offer an alternative to current methods of delivering therapeutic agents to the skin and other niches in the body. Moreover, the approach presented in this thesis investigates the effect this delivery might have on the natural skin microbiome and vice versa. This investigation might allow to understand the potential of my approach in a complex environment of the skin and make necessary changes to minimize the alteration to the natural skin microbiome while keeping the therapeutic efficacy.

2 Research Objectives

In this research, my goal was to develop a new methodology of delivering therapeutic agents to treat different skin conditions. Specifically, my main aim was to develop an engineered bacterium that proliferates on the scalp and continuously secrets a therapeutic agent. This novel approach is meant to resolve some of the limitations which current solutions possess (as previously explained in the introduction), potentially creating a therapeutics delivery approach that is continuous and effective on the one hand and hassle-free for the user on the other.

In order to develop this methodology, my research focused on the following objectives:

2.1 Finding a suitable microbiome member that will meet the necessary demands of my therapeutics delivery approach (e.g., secretion ability, prone to genetic manipulations and non-toxicity).

2.2 Prove the ability to express and secrete an active therapeutic agent in the engineered microbiome member described.
I chose, as a proof of concept, to focus this aim on a specific skin condition (MPHL).

2.3 Find a feedback system for the stability and viability of natural and engineered microbiome. This system should also provide a method to detect heterologous protein production of the engineered microbiome member in the native environment (i.e., on the skin). To that end, I employed next-generation sequencing and imaging assays to quantitatively and spatiotemporally track both the engineered bacteria and the natural biome.

3 Materials & Methods

3.1 Bacterial Growth Medium

- Lysogeny broth (LB): 1% Bacto™ tryptone (Becton Dickinson), 1% NaCl (Bio-Lab) and 0.5% Bacto™ Yeast Extract (Becton Dickinson). Addition of 1.5% Bacto™ Agar (Becton Dickinson) is necessary for agar plates.

- Minimal growth medium for bioassay (BA): 0.05% Bacto™ tryptone, 0.58% NaCl (Bio-Lab), 0.05M $MgSO_4$ (Merck), 1% phosphate Buffered Saline (Biological industries) and 0.03% Glycerol (Gadot).

- Recovery Medium for *E.Coli* Top10 transformations (SOB): 2% Bacto™ tryptone, 0.058% NaCl, 0.5% Yeast Extract and 0.019% KCl (Merck).

- Media and buffers used in *B. subtilis* RIK1285 transformation:

    - SPI salts: 0.2% $(NH_4)_2SO_4$ (Merck), 1.4% K_2HPO_4 (Merck), 0.6% KH_2PO_4 (Carlo Erba Reagents), 0.1% Na-Citrate·$2H_2O$ (Spectrum) and 0.02% $MgSO_4 \cdot 7H_2O$ (Alfa Aesar).
    - 10% Bacto™ Yeast Extract.
    - 50% Glucose (Sigma-Aldrich).
    - 50 mM $CaCl_2$ (Merck).
    - 250 mM MgCl2 (Merck).
    - 100 mM EGTA {ethylene glycol bis (β-amino ethyl ether)-N,N,N',N'-tetra- acetic acid} (Strem chemicals) adjusted to pH 7.0 with NaOH (Bio-Lab).

- Ampicillin, Kanamycin, and Chloramphenicol were used as selections antibiotics (Sigma-Aldrich).

3.2 Bacterial Strains

- *E.coli* Top 10 (Genotype - F- mcrA Δ(mrr-hsdRMS-mcrBC) ϕ80lacZΔM15 ΔlacX74 nupG recA1 araD139 Δ(ara-leu)7697 galE15 galK16 rpsL(StrR) endA1 λ-) was used for DNA transformation and plasmid propagation (Invitrogen). DNA was transformed using a standard heat shock transformation, after which the bacteria were grown overnight at 37°C on an LB agar plate containing the appropriate selection antibiotics.

- *E.coli* Stellar™ Competent Cells (Genotype - F–, endA1, supE44, thi-1, recA1, relA1, gyrA96, phoA, Φ80d lacZΔ M15, Δ (lacZYA - argF) U169, Δ (mrr - hsdRMS - mcrBC), ΔmcrA, λ–) were used for plasmid propagation when preparing the plasmid library aimed for 3α-HSD secretion (Takara) [26].

- *Bacillus Subtilis* RIK1285 (Genotype - Marburg 168 derivative: *trpC2, ys1, aprEdelta3, nprR2, nprE18*) was used as an expression and secretion organism, as well in the skin microbiome sequencing and imaging experiments (Takara). DNA was transformed following the protocol described in the literature [27].

3.3 Kits

- Wizard® SV Gel and PCR Clean-Up System (Promega) used for DNA purification from PCR reaction mix and agarose gels.

- NucleoSpin® Plasmid EasyPure (MACHEREY-NAGEL) was used for plasmid purification. As a preliminary step for *B. subtilis*, the cells were incubated with 1% lysozyme (Sigma-Aldrich) [27].

- *B. subtilis* Secretory Protein Expression System (Takara) was used to obtain a library of 173 different signal peptides (SP).

- In-Fusion® HD Cloning Plus (Takara), used to clone the different SP variants into the pBE-S plasmid, as well as the cloning of the Akr1c14 gene.

- NucleoBond® Xtra Midi plus EF (MACHEREY-NAGEL) was used to purify plasmids from *E.coli* Stellar™ cells to produce the plasmid library aimed for 3α-HSD secretion.

- Enhanced chemiluminescence kit (ECL) kit (Thermo) for visualization of western blot membranes.

- Kits used to Purify DNA from skin swab samples:

    - PureLink™ Microbiome DNA Purification Kit (Invitrogen)
    - DNeasy PowerSoil Kit (QIAGEN)

3.4 Vectors

3.4.1 pBE-S

A 5938 bp plasmid that is aimed to secrete proteins from *Bacillus Subtilis*. The gene that encodes the protein aimed to be secreted (i.e., the Akr1c14 gene encoding the 3α-HSD enzyme) is cloned downstream to a signal peptide. The sequence for the Akr1c14 (gene synonym for akr1c9) was taken from the literature, ordered as a gBlock® (IDT) and cloned into the pBE-S plasmid using the In-Fusion® cloning method [28]. This signal peptide can be one out of 173 variants that were ordered, as can be seen in figure 3.1 (Takara) [27]. These different variants of SP were cloned into the pBE-S plasmid using the In-Fusion® method as well.

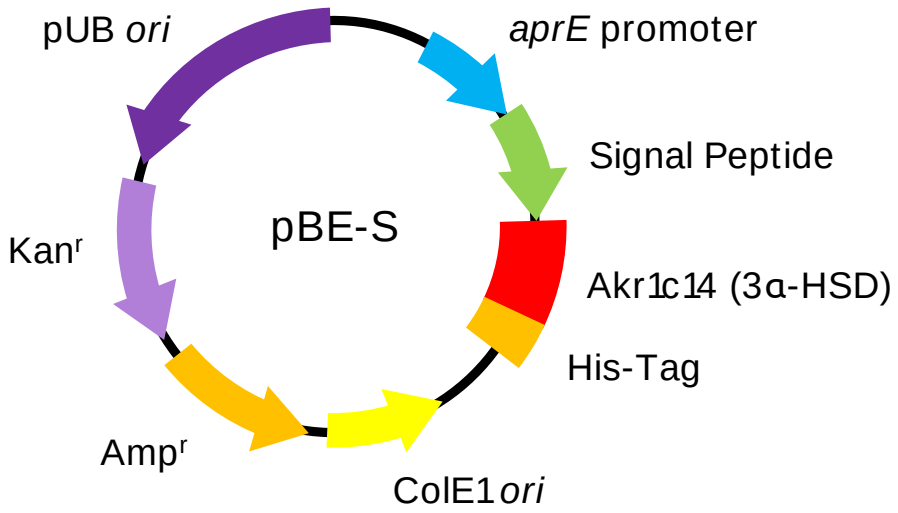

Figure 3.1 *pBE-S. This plasmid contains an aprE promoter, signal peptide region into which one of 173 signal peptides is introduced using an In-Fusion® reaction, an MCS into which the Akr1c14 gene was cloned followed by an HIStag domain used to identify the fused protein. As illustrated in this map, this plasmid also contains the colE1 origin of replication (ori) and an Amp^r gene (ampicillin resistance gene) aimed to be functional in E.coli. Moreover, this plasmid contains a pUB ori and a Kan^r (kanamycin resistance gene) aimed to be functional in B. subtilis [27].*

3.4.2 pBS3Clux

To establish a method analyzing skin microbiome and the effects of the addition of an engineered member of the microbiome to the skin, pBS3Clux was ordered (addgene). This Plasmid contains the luciferase reporter gene (*luxABCDE*), has selection genes for both *E.coli* (used for plasmid propagation) and *B. subtilis*, and undergoes integration into the *sacA* locus of *B. subtilis* as illustrated in figure 3.2 [29]. RFP (found in the original plasmid) was replaced in with a strong constitutive promoter (Pveg, which was obtained from the iGEM registry) cleaving the plasmid with the *EcoRI-HF®* and *SpeI-HF®* restriction enzymes (NEB), and a subsequent ligation [30].

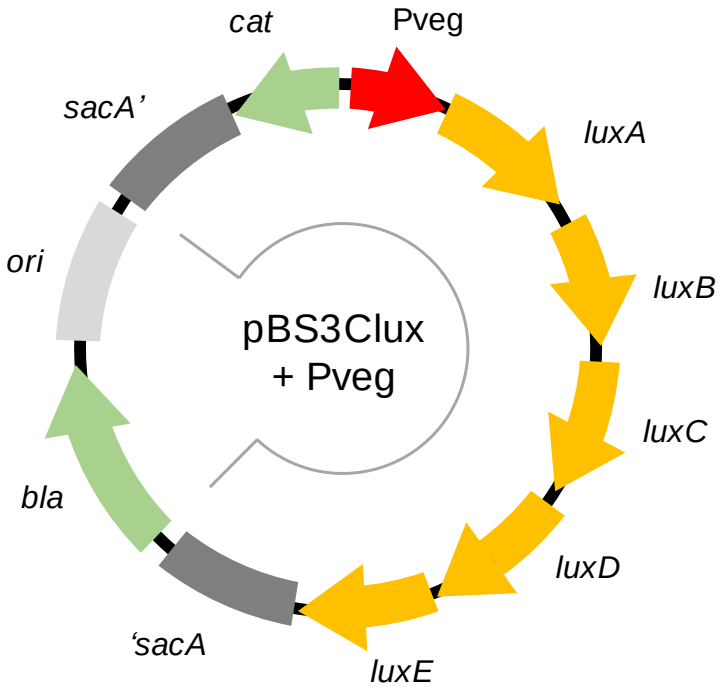

Figure 3.2 *pBS3Clux + Pveg. The part that undergoes integration into the genome is marked by a thin line within the plasmid [29]. The plasmid also contains the bla gene (ampicillin resistance) and an ori for selection in E.coli. Moreover, a cat gene (chloramphenicol resistance) is located within the part that undergoes integration into the B. subtilis genome for selection of positive clones. Pveg, a strong constitutive promoter, was cloned upstream to the luxABCDE gene.*

3.5 DHT Actfivity assay

3.5.1 Secretion Of 3α-HSD – A Model for Developing a Therapeutic, Microbiome-Based Agent

Here, the creation of a chimeric protein is described. This chimera consists of 3α-HSD (heterologous enzyme) fused to a library of 173 SP domains (from secreted endogenous proteins) from SEC, TAT, and unknown secretion pathways. The library was screened for the best possible secretion signal for 3α-HSD (i.e., will yield the most active, secreted protein).

3.5.1.1 Creation Of 3α-HSD Secreting *B. subtilis* Library

A DNA fragment of akr1c14 variant of the 3α-HSD gene (a gene synonym for akr1c9, ordered from IDT) was incorporated into pBE-S plasmid following a standard In-Fusion® cloning protocol [28] [27]. Next, the plasmid was linearized by cleaving it with *MluI-HF*® (NEB) and *Eco52I* (*EagI-HF*® ordered from NEB) restriction enzymes, and the 173 variant SP mix was inserted using a standard In-Fusion® protocol [27]. The resulting reaction mixture was transformed into *E. coli Stellar*™ cells to create a library with a high copy of plasmid DNA (i.e., plasmid propagation). The resulting 1960 colonies were scraped from the agar plates and the DNA was purified using the NucleoBond® Xtra Midi plus EF kit to achieve a high DNA complexity. This plasmid library was then transformed into *B. subtilis* RIK1285, yielding 1152 colonies. Separate 80% Glycerol (Bio-Lab) 20% LB stabs were created for each clone in the library, and stored in -80°C.

3.5.1.2 Verification of Enzymatic Activity Of 3α-HSD by Measurement of Decrease Rate of NADPH Fluorescence Over Time in The Presence of 5α-DHT

To efficiently verify an adequate expression and secretion of 3α-HSD for each clone, an assay in which the degradation rate of the cofactor, NADPH, is measured was developed, as illustrated in figure 3.3.

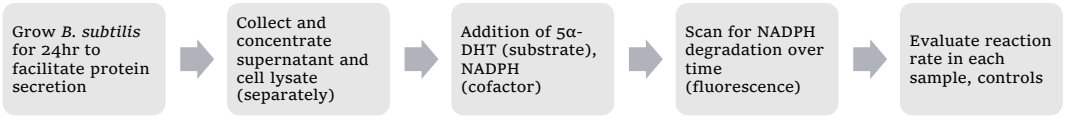

Figure 3.3 *Scheme of the 3α-HSD library screening.*

Individual colonies from the 3α-HSD secreting *B. subtilis* RIK1285 library were grown for 24 hours in BA with 5% LB and 0.001% Kanamycin, 37°C and 250 rpm shanking. Next, samples were centrifuged for 10 min. at 17 ×g for the cell supernatant (i.e., the fraction in which secreted proteins are located) to be isolated. Incubation time, as well as the other properties of the assay (e.g., the *B. subtilis* strain), were determined according to preliminary calibration experiments and the literature, with the aim to achieve high concentrations of the secreted protein in the medium [31].
Fixed incubation time was previously compared to more precise harvesting methods (based on a specific growth phase), with the conclusion that harvest and cultivation settings have no significant effect on the activity results obtained in the assay [32].

200 µl of supernatant from each cloned colony, control supernatants (*B. subtilis* clone without the 3α-HSD) were transferred into new separate wells (in ice and covered with foil), duplicate for each condition. These wells were supplemented with 200 µM of NADPH (Sigma-Aldrich), dissolved in NaOH, and 150 µM 5α-DHT, dissolved in Methanol (Gadot), in addition to negative control supernatants to which NADPH, 5α-DHT, or both were not added. Fluorescence was then measured every minute for 5 hours at 340nm excitation, 450nm emission – indicating NADPH concentration in sample [13]. The reaction took place at 37°C, imitating physiological conditions.

Analysis of all measurements was carried out as follows. An average of the repeated measurements was plotted (fluorescence as a function of time) and a linear trend line was fitted (i.e., least squares regression fitting). The linear slope of fitted line received from 10 min. into the reaction until 56 min. into the reaction (same duration for each colony) was calculated (for positive clones and negative controls without the 3α-HSD gene). Moreover, the coefficient of determination (R^2) was measured for each fitted line.
In Figure 3.4, I plot a degradation curve for a secreting strain as compared with a non-secreting control (negative control) as an example.

The plot shows a significantly more rapid decline (as exemplified by the fit) for the secreting strain indicating a more rapid utilization of NADPH, which supports active secretion of 3α-HSD.

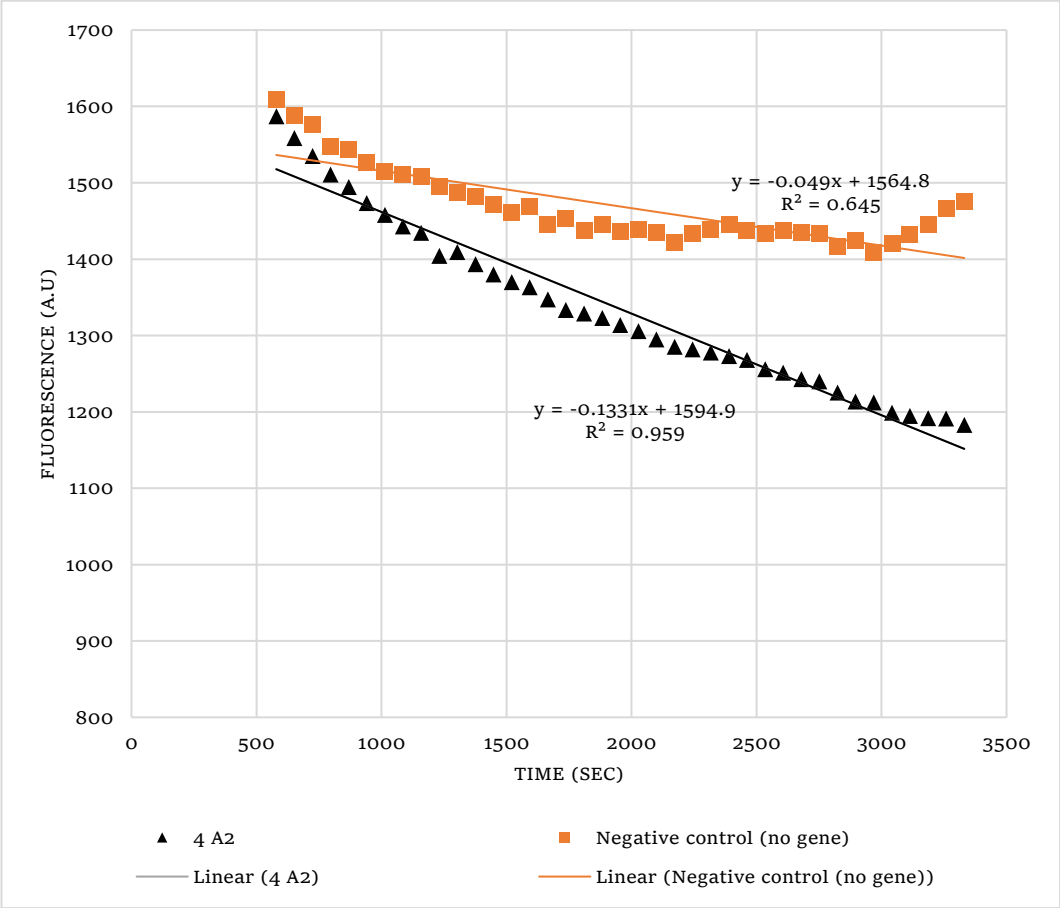

Figure 3.4 *An example of linear least squares regression fitting of fluorescence as a function of time. This figure presents a secreting strain (labeled as 4 A2 in table 4.1) and its negative control (represented in grey). The linear slope, as well as the coefficient of determination (R^2) are also presented in this chart for each colony.*

This slope is a direct indicator of the degradation rate of NADPH in the cells supernatant. A steeper slope and hence increased NADPH degradation rate is an indicator of secreted 3α-HSD activity in the *B. subtilis* cells. Finally, colonies were sequenced, and the unique SP was matched for each colony.

3.6 Western Blotting Specific Qualitative Analysis of Secretion

In order to verify the secretion of 3α-HSD from *B. subtilis*, a western blot analysis was designed with the aim to compare the anti-HIS signal of the supernatant with the cell lysate in a clone that presented positive 3α-HSD activity in the assay described in section 3.5.1.2, and with negative controls.

First, *B. subtilis* tyrA-3α -HSD variant (labeled 9 h5 in table 4.1) expressing the akr1c14 gene conjugated to a HIStag domain in the c-terminal end (as can be seen in figure 3.1), were grown for 24 hours in LB and 0.001% Kanamycin, 37°C and 250 rpm shanking.
A clone containing no 3α-HSD and a clone without an SP fused to the 3α-HSD gene were also grown in the same manner (negative controls). The clone without an SP fused to the 3α-HSD was created using PCR amplification that excluded the SP. Cell lysates were collected after the cell debris had been resuspended in PBS 1X (Biological Industries) and underwent a standard sonication protocol.

In the following step, supernatants and cell lysates were concentrated (separately) using the 10K Amicon® Ultra filters (Merck) size exclusion columns. 10 µl of the concentrated protein solutions were mixed with 30 µl of the sample buffer and denaturated for 5 minutes at 98˚C. The samples were centrifuged for 5 minutes at 17,000 xg and resolved by electrophoresis using a 12% SDS- polyacrylamide gels. The resolving gel solution was poured between 2 thin glass plates with 1.5mm distance in-between, following the addition of isopropyl alcohol (Gadot) that was poured on top for tightening.
The gel was left for 45 minutes to polymerize, after which the isopropyl alcohol was removed, and the stacking gel was poured and left for 25 minutes to polymerize. The gel was loaded with the samples together with controls and placed in the running chamber, covered with running buffer. The positive control for HIStag detection used in this assay was the His6-eIF4HII protein (human, 29 kDa) that was purified by a His-trap column, generously donated by Prof. Amit Meller's Lab (Technion).

The protein ladder that was used is Blueye prestained protein ladder (Jena Bioscience). The gel was run for 90-120 min. at 110-120 V.

For specific qualitative detection of HIS-tagged protein, gels were electro-transferred to a nitrocellulose membrane (Whatman) in a chamber filled with transfer buffer and surrounded by ice, at 200 mA for 2 hr. The transfer was verified using Ponceau-S staining.
In the following step, TBS-T buffer (TBS with 0.1% Tween-20, Acros) with 5% Blotting-Grade blocker (Bio-Rad) was added to block the membrane for a 1 hr. incubation on a shaker (room temperature).
The membrane was then incubated with the primary antibody, Anti-6X His tag® antibody [HIS.H8] (Abcam) diluted 1:1000 in blocking solution TBS-T with 5% Blotting-Grade blocker, overnight on a shaker at 4˚C. The membrane was then washed three times for 3 minutes each with TBS-T buffer.
The membrane was incubated with an HRP-conjugated anti-Mouse antibody (Amersha) diluted 1:10,000 in TBS-T, with subsequent incubation in a shaker for 1 hr. (room temperature).
In the following step, the membrane was washed three times for 3 min. each with TBS-T buffer.
Lastly, the membrane was visualized with enhanced chemiluminescence (ECL) kit (Thermo) using ImageQuant LAS4000 (GE-Healthcare Life Sciences).

3.6.1 Solutions & Buffers

- Sample buffer: Laemmli Sample Buffer 4x (Bio-Rad), mixed with 10% β-mercaptoethanol (Sigma-Aldrich).

- Lower buffer (×4): 1.5M Trizma® base (Sigma-Aldrich) pH=8.8 adjusted with HCl (Merck), 0.4% (v/v) SDS (BIOLOGYCAL).

- Upper Buffer (×4): 0.5M Trizma® base (Sigma-Aldrich) pH=6.8 adjusted with HCl (Merck), 0.4% (v/v) SDS (BIOLOGYCAL).

- Lower gel (resolving gel) 12%: 25% (v/v) Lower buffer (×4), 33.3% (v/v) Acrylamid:bisacryl (29:1) (Sigma-Aldrich), 1% (v/v) Ammonium persulfate (Sigma-Aldrich), 0.125% (v/v) TEMED (ALFA AESAR).

- Stacking Gel (upper gel) 6%: 25% (v/v) Upper buffer (×4), 6% (v/v) Acrylamid:bisacryl (29:1), 1% (v/v) Ammonium persulfate (Sigma-Aldrich), 0.15% (v/v) TEMED (ALFA AESAR).

- Running buffer: 0.3% Trizma® base, 1.44% glycine (Sigma-Aldrich), 0.1% (v/v) SDS.

- Ponceau-S: 5 ($\frac{gr}{lit}$) Ponceau-S (Sigma-Aldrich), 1% (v/v) Glacial acetic acid (Frutatom).

- TBSX10 (concentrated Tris-buffered saline) buffer: 200mM Tris-HCl pH=7.6, 1.37M NaCl (Bio-Lab).

- TBS-T buffer: 10% (v/v) TBS X10, 0.1% (v/v) Tween-20 (Acros).

3.7 Skin Microbiome Research Toolbox

The *B. subtilis* RIK1285 was transformed to express the pBS3Clux + Pveg plasmid (figure 3.2) and was used in both complementary assays described below. These assays may answer the needs that were presented in recent publications for visualization techniques of the skin microbiome and availability of experimental data at several timepoints [20]. Also, these assays may provide tools for tailored analysis the skin microbiome.

3.7.1 Imaging Assay

I aimed to create a tool that will aid in the investigation and further characterization of *B. subtilis* RIK1285 + pBS3Clux + Pveg (engineered microbiome member).
This assay should be complementary to the Next Generation Sequencing assay described in section 3.7.2.

3.7.1.1 In-Vitro Imaging Assay

Initially, agar plates containing the appropriate selection antibiotics were inoculated and grown overnight with the following strains:

- *B. subtilis* RIK1285 + pBS3Clux + Pveg (agar plate containing CM)

- *B. subtilis* RIK1285 + pBE-S (agar plate containing KAN) – negative control

The plates were taken out and read for bioluminescent signal using ImageQuant™ LAS 4000 (GE) at 10-second intervals of continues exposure (i.e., images were taken at 10 seconds, 20 seconds and up).

3.7.1.2 *Ex-Vivo* Imaging Assay

In this assay, it was aimed to image the *B. subtilis* RIK1285 + pBS3Clux + Pveg on the skin, measuring its ability to grow, proliferate and express the heterologous bioluminescent protein in its natural environment. The following strains were grown in LB overnight with 0.001% (v/v) of the appropriate selection antibiotic (twice for each strain):

- *B. subtilis* RIK1285 + pBS3Clux + Pveg (LB containing CM)

- *B. subtilis* RIK1285 + pBE-S (LB containing KAN) – negative control

One out of two tubes for each strain was centrifuged for 5 min. at 5000 rpm to remove residues of the medium from the cells (i.e., LB), following resuspension with PBS 1X (same volume as LB).

50 µl of the bacteria were spread on a porcine ear skin patch of roughly 4 cm^2, one patch with bacteria in PBS and the other with bacteria in LB for each strain. PBS was used as a neutral buffer – to analyze the growth of the bacteria on the skin without the addition of growth medium. These patches were incubated at 37°C to imitate the natural porcine ear skin temperature [33]. The patches were taken out at 1,3,6,8,9 and 24 hr. after inoculation and read for bioluminescent signal using ImageQuant™ LAS 4000 (GE) at 20 second intervals of continues exposure (i.e., images were taken at 20 seconds, 40 seconds and up).

3.7.2 Next Generation Sequencing Assay

3.7.2.1 Sampling Method and Purification Kit Selection Calibration Experiment

Initially, two sampling methods were tested. In the first method, a whole mouse back was trimmed and swabbed ten times using buccal swabs (isohelix) which were dipped into a sterile swab rewetting solution - 0.15M NaCl and 0.1% Tween 20 (Sigma-Aldrich) [34]. In the second method, skin patch of $4 \times 1.5\ cm^2$ were cut from a trimmed mouse back and then swabbed as explained. The aim of the second swabbing method was to allow the incubation of skin samples over a period of time (as describred in section 3.7.2.2), which is not technically possible when using a whole animal. In total, four mice were used for this experiment: two uncut mice that were swabbed twice each. Two additional mice's skin were cut for skin patches (two separate patches from each mouse).

DNA from each sampling method was purified using two different purification kits that were compared: PureLink™ Microbiome DNA

Purification kit and the DNeasy PowerSoil kit. I sought to compare two kits and check if any difference exists.

Purified DNA was then amplified for the V3-V4 variable regions of the 16s rRNA, using the standard primer set described in the literature [35]. 20 ng of the template DNA were taken into the PCR reaction, together with 20% (v/v) Q5® High-Fidelity 2X Master Mix (NEB), 2% (v/v) 10mM dntp (agilent), 0.5% (v/v) of 100 μM of each primer (IDT), 1% (v/v) Q5® High-Fidelity DNA Polymerase (NEB), 3% (v/v) Dimethyl Sulfoxide (DMSO) (Merk) and supplemented with ultra-pure water (BIOLOGYCAL IND.) for a 50 μl reaction. Further sequencing steps of the samples were made in accordance with the Illumina Miseq sequencing guidelines [35].

Bioinformatic analysis was performed by Oz Solomon using the QIIME™ open-source bioinformatics pipeline [36].
Briefly, adapters were trimmed from the reads using cutadapt and aligned against the bacterial reference 16S rRNA sequences (GreenGenes version 13.8) using QIIME™ [37]. Reads with higher than 97% identity were clustered together. Different sequences were compared against the reference taxonomy, and operational taxonomic units (OTU) were picked using QIIME™. OTUs were averaged among samples at the phyla level. Alpha diversity score (chao1) was calculated using QIIME™.

3.7.2.2 Different Condition Sampling

In the following step, I chose to work with mice back skin patches and the PureLink™ Microbiome DNA Purification kit. This step aimed to examine the skin microbiome composition with the introduction of different mediums and buffers. Moreover, I sought to find out how the introduction of an engineered member of the microbiome (*B. subtilis*) affects this composition and achieve an initial understanding of the relationship between natural and engineered skin microbiome members over time.

Skin patches were supplemented as described in the following list, two patches from different mice for each condition (biological repeat):

- Native skin patches samples (no addition)
- 50 µl of LB
- 50 µl of Pluronic® F-127 18% (Sigma-Aldrich, provided by the Mizrahi Lab, Technion)
- 50 µl of native *B. subtilis* RIK1285, 0.1 O.D, in LB.
- 50 µl of *B. subtilis* RIK1285 + pBS3Clux + Pveg, 0.1 O.D, in LB.
- 50 µl of *B. subtilis* RIK1285 + pBS3Clux + Pveg, 0.1 O.D, in 18% Pluronic®.

It was documented in the literature that the density of bacterial strains on the scalp is within the $(1.4 \times 10^3 - 2.2 \times 10^5) \frac{CFU}{cm^2}$ range (depending on the strain) [38]. In my described experiment, 50 µl of bacterial medium containing 0.1 OD, spread on an area of $4 \times 1.5\ cm^2$ equals to roughly $7 \times 10^4 \frac{CFU}{cm^2}$ of *Bacilli* [39], in line with the physiological range shown above.

The skin patches (biological repeat for each condition) were incubated at 37°C (in accordance with mice skin temperature documented in the literature) with 100 µl PBS1X poured into the surrounding of the patches for moisture [40].

Sampling was made using skin swabs, as described in section 3.7.2.1, at 0, 3 and 24 hr. (separate swab area for each time point). Two swab samples were taken for each condition (biological repeats).

DNA from each sampling method was purified using the PureLink™ Microbiome DNA Purification kit. Purified DNA was then amplified for the 16S rRNA V1-V3 variable regions using the set of primers shown in table 3.1 (together with the standard Illumina adaptors) [35] [41].

Sequencing the V1-V3 regions was shown to be the most accurate for skin microbiome classification [20]. 12.5 ng of the template DNA were taken into the PCR reaction, together with 20% (v/v) Q5® High-Fidelity 2X Master Mix (NEB), 2% (v/v) 10mM dntp (agilent), 0.5% (v/v) of 100 µM of each primer (IDT), 1% (v/v) Q5® High-Fidelity DNA Polymerase (NEB), 3% (v/v) Dimethyl Sulfoxide (DMSO) (Merk) and supplemented with ultra-pure water (BIOLOGYCAL IND.) for a 50 µl reaction. Bioinformatic analysis was performed by Oz Solomon using the QIIME™ open-source bioinformatics pipeline, as previously described.

Table 3.1 *Primers used for the V1-V3 amplification.*

Name	**Sequence**
F27 with adapters	TCGTCGGCAGCGTCAGATGTGTATAAGAGACAGAGAGTTTGATCCTGGCTCAG
R534 with adapters	GTCTCGTGGGCTCGGAGATGTGTATAAGAGACAGATTACCGCGGCTGCTGGC

4 Results

4.1 3α-HSD Activity in Supernatant

As previously mentioned in the introduction, to obtain an optimal secretion of heterologous proteins from *B. subtilis*, there's a need to tailor a specific signal peptide to the secreted protein. This specific tailoring might result in a correctly folded protein with significant activity [17]. As previously described in section 3.5, I built a library of 173 signal peptides conjugated to the 3α-HSD gene and scanned for secreted 3α-HSD activity.

To verify the enzymatic activity of 3α-HSD, I chose to measure the levels of the cofactor of the enzymatic reaction, NADPH, over time. It is believed that the secretion of the enzyme into the medium will increase the NADPH degradation rate in the medium (as explained section 3.5.1.2) [13].

In table 4.1, I summarize the slopes of the measured NADPH degradation, reflecting 3α-HSD activity (based on NADPH degradation rate), together with the SP which was responsible for the secretion according to sequencing results. Folds of activity is defined as the NADPH degradation rate of the variant divided by the degradation rate of the non-secreting phenotype (average control). The standard deviation and the coefficient of determination (R^2) are also presented in this table. The assumed secretory pathway is also shown for each of the 40 distinct SP scanned. The average slope of the colony without the 3α-HSD gene inserted (negative control) is also shown (average of four biological repeats).

Table 4.1 *Scanning results of the SP library. The scan is of an SP library that is fused to the Akr1c14 gene. Each gray bar corresponds to the fold activity measured for the SP variant labeled. The slope ($-\frac{1}{a.u}$) of each colony, the coefficient of determination (R^2), the standard deviation, folds of activity over the control, the sequenced variant of SP and the secretion pathway are presented.*

Colony Code	Slope (-1/a.u)	R^2	Standard Deviation	Folds Over Control	SP	Secretion Pathway
13 G3	0.1854	0.984	0.0408	2.3	yfhK	SEC
11 H3	0.1672	0.970	0.0151	2.1	yfkD	SEC
13 E1	0.1664	0.974	0.0119	2.1	tasA	SEC
12 G3	0.1641	0.949	0.0095	2.1	sleB	SEC
13 G6	0.1633	0.967	0.0101	2.1	wapA	SEC
9 H5	0.1612	0.958	0.0068	2.0	tyrA	SEC
9 A4	0.1583	0.980	X	2.0	ybbR	SEC
9 F6	0.1581	0.977	0.0036	2.0	yjcN	SEC
11 A4	0.1544	0.976	0.0046	2.0	ydjM	SEC
9 H2	0.1475	0.977	0.0026	1.9	yjfA	SEC
12 F4	0.1463	0.956	0.0041	1.8	sacC	SEC
9 A2	0.1406	0.898	X	1.8	yurI	SEC
5 A4	0.136	0.963	0.0064	1.7	penP	SEC
11 A2	0.1348	0.896	0.0111	1.7	aprE	SEC
3 A4	0.1348	0.948	0.0042	1.7	ylxF	SEC
12 A4	0.1342	0.957	0.0124	1.7	aprE	SEC
4 A2	0.1331	0.959	0.0001	1.7	ykwD	SEC
6 A2	0.1331	0.953	0.0039	1.7	aprE	SEC
10 A4	0.1293	0.956	0.0014	1.6	aprE	SEC
5 A3	0.1273	0.917	0.0139	1.6	yrvJ	SEC
5 A2	0.1253	0.940	0.0097	1.6	aprE	SEC
13 A2	0.1243	0.975	0.0067	1.6	ydhT	SEC
9 G3	0.1224	0.953	0.0034	1.5	yhfM	SEC
4 A4	0.1222	0.966	0.0070	1.5	phoB	SEC
2 A3	0.1203	0.942	0.0060	1.5	yfkN	SEC
7 A2	0.1203	0.920	0.0064	1.5	yolC	SEC
11 A3	0.1128	0.829	0.0079	1.4	yurI	SEC
6 A3	0.1099	0.924	0.0256	1.4	dltD	TAT
3 A2	0.1089	0.876	0.0032	1.4	ylxF	SEC
2 A4	0.108	0.952	0.0215	1.4	pbpB	Undocumented
8 A2	0.106	0.895	0.0322	1.3	yjcM	SEC
8 A4	0.1038	0.918	0.0021	1.3	ydhT	SEC
1 A3	0.1026	0.924	0.0177	1.3	aprE	SEC
13 A3	0.0996	0.880	0.0179	1.3	sacB	SEC
10 A3	0.0981	0.895	0.0145	1.2	phrF	SEC
3 A3	0.0967	0.910	0.0019	1.2	aprE	SEC
12 A3	0.0939	0.829	0.0171	1.2	ykvV	SEC
13 A4	0.0881	0.900	0.0103	1.1	aprE	SEC
4 A3	0.0867	0.859	0.0028	1.1	ydbK	SEC
10 A2	0.0755	0.952	0.0373	1.0	phrK	SEC

Average control (no gene): $(0.0791 \pm 0.0296) - \frac{1}{a.u}$

The results presented in table 4.1 indicate that secretion of an active 3α-HSD might be increased by up to 2.3 folds over control and 1.6 folds over backbone aprE (average value, as shown below). Moreover, 9 out of the 40 colonies scanned present a 2-fold activity over the control. I believe that this indicates the secretion of an active 3α-HSD to the medium in these clones. The average coefficient of determination (R^2) for the 40 tested colonies is 0.934 ± 0.0402, indicating a strong correlation in the linear least squares regression fitting between the observed values and the predicted ones.

In figure 4.1, the slopes of the measured NADPH degradation of the colonies with the backbone SP aprE mutant are presented, compared with the baseline of the control as presented in table 4.1 (cells without the gene inserted – orange line). As expected, the prevalence of this variant is the highest – 1 out of 7 colonies scanned from my data (table 4.1). There is no statistically significant difference between the samples. The average NADPH breakdown measured for these 6 Colonies is 0.1178±0.0183, which is significantly different from the average control, $p < 0.003$ (T test). These results indicate that the assay might be reproducible.

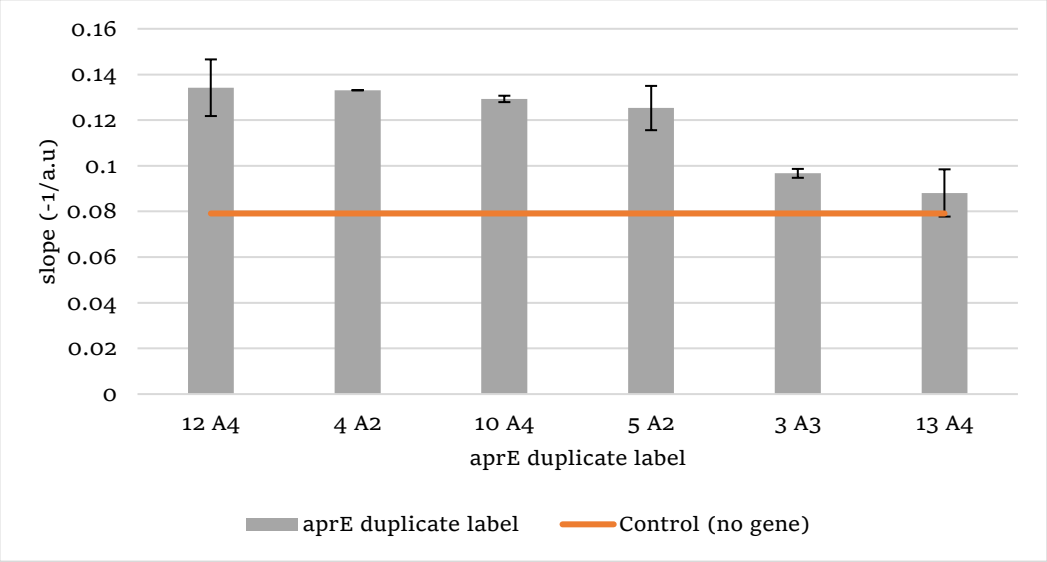

Figure 4.1 *Average slope for aprE screened colonies. Non-secreting phenotype (average control) represented by an orange line. The bars represent the standard deviation for each sample, as shown in table 4.1.*

4.2 3α-HSD Secretion Verification (Western Blotting Specific Qualitative Analysis)

In order to illustrate and further verify the secretion of the 3α-HSD from *B. subtilis*, a western blot analysis was performed on a representative sample (a secreting colony labeled 9 h5 in table 4.1). The Western blot membrane results, presenting the different samples analyzed as previously described in section 3.6, can be seen in figure 4.2. The expected band for 3α–HSD is 37 kDa in size [42].

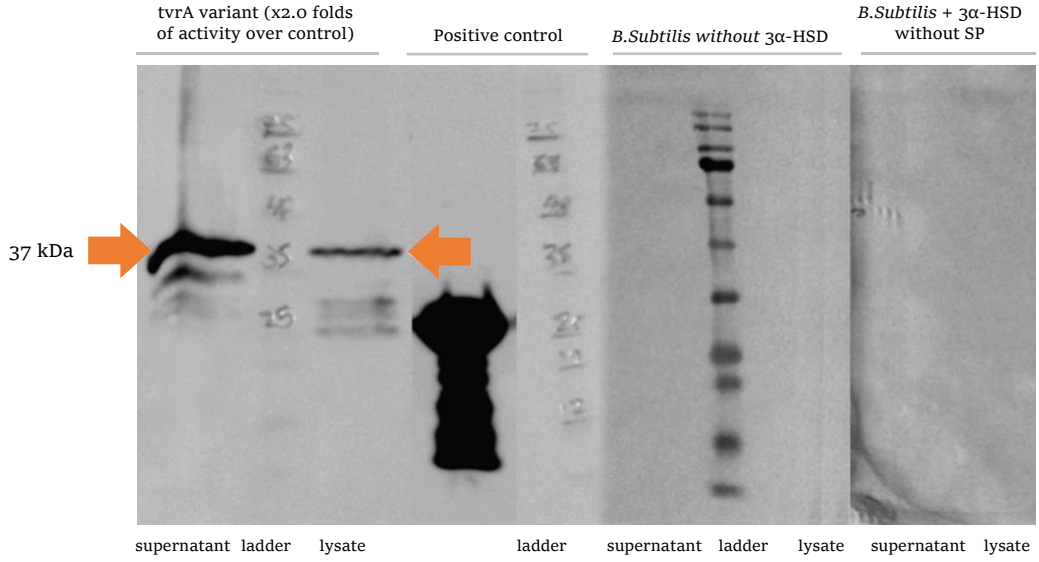

Figure 4.2 *Western blot results depicting the supernatant of the tyrA-3α–HSD variant (left band), the cell lysate of the tyrA-3α–HSD variant (second from left), positive control (a 29 kDa protein fused to a His-tag domain – third from left) and negative controls: B. subtilis without SP fused 3α–HSD (right band).*

Figure 4.2 presents a strong 37 kDa band corresponding to 3α-HSD in the supernatant as well as in the cell lysate. This result supports the results of the 3α-HSD activity assay (i.e., an active 3α-HSD can be found in the cell supernatant). Weak non-specific secondary bands appear for this strain as well. These bands are likely caused by a natural protease protein digestion or by a higher than required primary antibody concentration [43].

Two additional variants were tested as controls. The first was *B. subtilis* without the 3α-HSD (served as a control in the 3α-HSD activity assay) and the second is a variant without SP fused to 3α–HSD. In both cases, no specific band was detected.

4.3 LC-MS Results for 5α-DHT

I next wanted to develop an orthogonal method for measuring 5α-DHT degradation, that could potentially be of use to test *in-vivo* samples. To that, I decided to employ LC-MS. This method is sensitive and accurate for the quantification of 5α-DHT [44] [45]. Dried samples of 5α-DHT were sent to The Mass Spectrometry Division at Bar-Ilan University and were analyzed using Q-TOF 6545 (High Resolution) LC-MS ESI (Agilent) by Dr. Michal Weitman.

In figure 4.3, LC-MS chromatograms for 5α-DHT ($C_{19}H_{30}O_2$, molecular weight 290.44) is presented [46].
The ionized 5α-DHT can be seen in this chromatogram as the highest peak. Due to time constraints, I was unable to send a supernatant to the LC-MS unit to further confirm the breakdown of 5α-DHT. However, the ability to detect 5α-DHT indicates that such an assay can indeed be complementary.

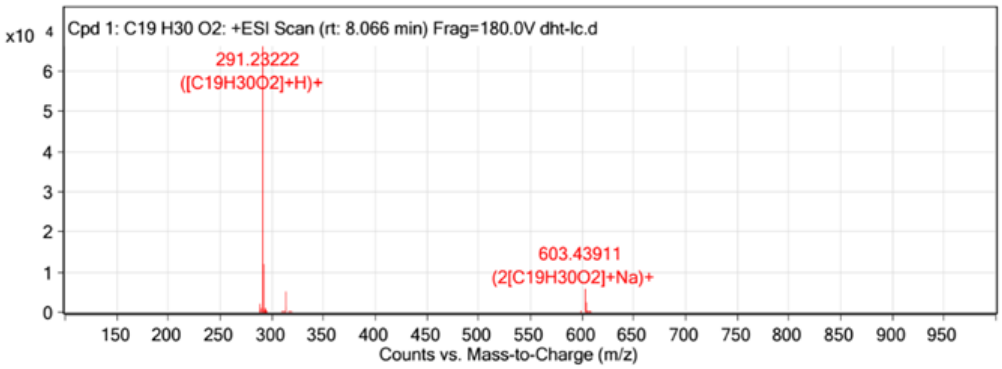

Figure 4.3 *LC-MS chromatogram for 5α-DHT.*

4.4 Skin Microbiome Research Toolbox

After the secretion of an active 3α-HSD from an engineered microbiome member was proven, I sought to examine the viability and heterologous protein production in the engineered microbiome member. Also, the effects that inoculation with an engineered microbiome member might have on the natural skin microbiome (and vice versa) were also aimed to be observed.

4.4.1 Imaging Assay

To investigate the viability and active heterologous protein expression of an engineered member of the microbiome, a substrate-independent marker (*luxABCDE)* was cloned into *B. subtilis* under a strong constitutive promoter (As described in section 3.4.2 and 3.7).
This construct allowed the independent investigation of the engineered population in the native environment. The assay was tested both *in-vitro* and *ex-vivo*.

4.4.1.1 In-Vitro Results

In figure 4.4, the imaging results of plates inoculated with *B. subtilis* expressing the *luxABCDE* cassette, as well as negative control (*B. subtilis* without *luxABCDE*) are presented. These two images are taken with the same exposure settings.

As seen in figure 4.4, only the *B. subtilis* strain that expresses the *luxABCDE* cassette emit a substantial bioluminescent signal, as expected.

B. subtilis RIK1285 + pBS3Clux + pVEG

B. subtilis RIK1285 (negative control)

Figure 4.4 *In-vitro imaging results. It can be seen from this figure that bioluminescent light is emitted only from the B. subtilis RIK1285 + pBS3Clux + Pveg strain (imaging and exposure setting are identical).*

4.4.1.2 *Ex-Vivo* Results

In figure 4.5, the imaging results from inoculated skin patches are presented.

All presented images were taken with the same exposure settings. After the verification of active heterologous protein production *in-vitro*, these properties were aimed to be observed *ex-vivo* on porcine ear skin patches (as previously explained in section 3.7.1).

As shown in figure 4.5, only the *B. subtilis* strain that expressed the *luxABCDE* cassette emits a bioluminescent signal, even after 1 hour of incubation. This signal increased over time, with a peak measured after 8 hours of incubation. The signal slightly decreased after 9 hours, with almost no signal emitted after 24 hours. I believe that this deterioration in growth is due to the loss of natural, physical properties of the skin (e.g., loss of hydration) that affected the viability of the microbiome (both native and engineered) [1].

The bioluminescent signal emitted from the engineered population was observed from both mediums tested, PBS 1X and LB, with a slightly stronger signal emitted from *B. subtilis* in PBS 1X. The growth in PBS1X is an indicator of natural growth and proliferation of the engineered *B. subtilis* on the natural resources available on the skin – the PBS1x does not contain any growth media [47].

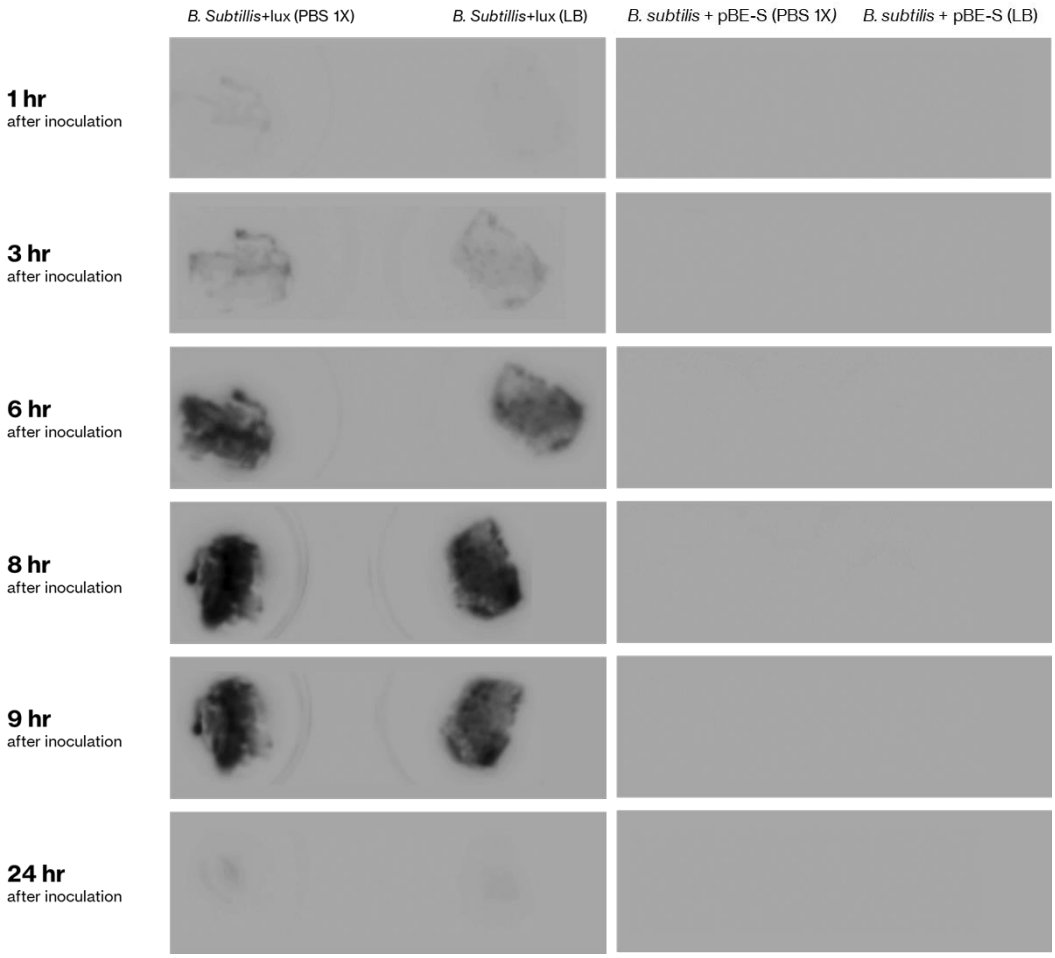

Figure 4.5 *Ex-Vivo Imaging Results. from left to right, the following strains are presented: B. subtilis RIK1285 + pBS3Clux + Pveg in PBS 1X, B. subtilis RIK1285 + pBS3Clux + Pveg in LB, B. subtilis RIK1285 + pBE-S (negative control) in PBS 1X and B. subtilis RIK1285 + pBE-S (negative control) in LB. It can be seen from this figure that bioluminescent light is emitted only from the B. subtilis RIK1285 + pBS3Clux + Pveg strain.*

4.4.2 16s Next-Generation Sequencing Assay

The substantial growth, proliferation and heterologous protein production in an engineered member of the microbiome (i.e., *B. subtilis*) were shown in the imaging assay. In the following step, it was sought to quantify the growth of the engineered member of the microbiome when it is introduced to the natural environment and observe the effect that this introduction in different mediums might have on the natural skin biota.

4.4.2.1 Sampling Method and Purification Kit Selection

As previously mentioned in section 3.7.2.1, the comparison of two different sampling techniques (swab sampling from a whole animal and swab sampling from skin patches) was performed. Skin patches were intended to be used in the further *ex-vivo* experiments since the incubation of a whole animal was not feasible. Cutting and disconnecting the skin patch might influence the skin microbiome composition. It was therefore sought to verify that this difference is not significant before perusing with working on skin patches.

Also, DNA from each sampling method was purified using two different purification kits that were compared. The DNeasy PowerSoil kit was used previously in the literature and is not specific for skin swab samples [48] [49] [50]. The PureLink™ Microbiome DNA Purification Kit is a dedicated kit for microbiome samples, with specific guidelines for purification of DNA from swab skin samples [51]. This kit is more specific and less time consuming and hence was preferred for the developed assay. The traditional kit (i.e., the DNeasy PowerSoil kit) and the newer, more specific kit (i.e., the PureLink™ Microbiome DNA Purification kit) were hence compared to verify that the difference is not significant.

The Chao 1 index, species richness estimator that estimates the total number of species present in a sample, is a standard estimator for the of the within-sample (alpha) diversity. The chao 1 index was included in the QIIME™ analysis performed to estimate the differences between the methods described [52].

The differences in the diversity of the sampling methods and different kits are presented in figure 4.6. From the results presented in figure 4.6, a prominent change is neither observed between the two kits, nor between the two sampling methods tested. The slight changes that are observed between the samples might be due to natural variability between different mice and swabs.

After no prominent change was observed between the sampling methods and purification kits tested, it was chosen to work with mice skin patches and the PureLink™ Microbiome DNA Purification kit.

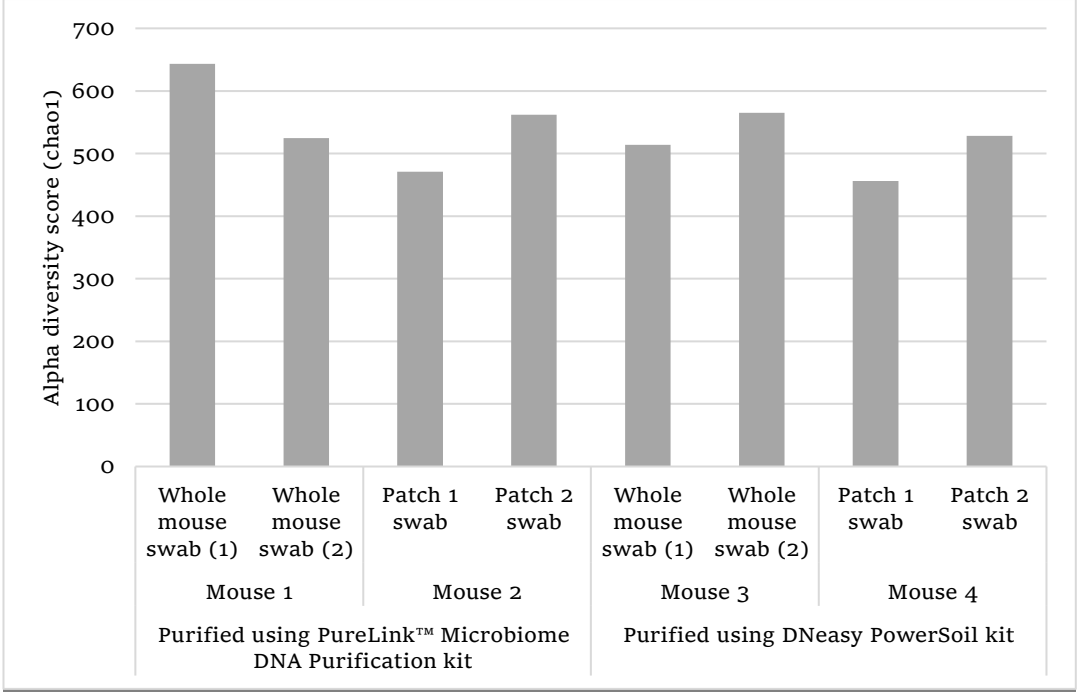

Figure 4.6 *Alpha diversity for different sampling methods, DNA purification kits, estimated by the Chao 1 index.*

4.4.2.2 Different Condition Sampling

Next, it was aimed to examine the permutations in the skin microbiome composition as a result of different mediums and bacterial strains applied.

The following figures (figures 4.7-4.9) present the phylum abundance in the samples collected. The major phylum groups presented in these figures are similar to the groups previously reported in mice [53].

At first, to establish a baseline, the native skin microbiome was tested. In figure 4.7, the relative phylum abundance of the native skin is shown at three-time points over 24 hours, for two biological repeats. For mouse 1, the phylum composition stays roughly the same for 24 hours. For mouse 2, there is a change in the phylum composition over time, but the composition is comparable to mouse 1. The small band of Firmicutes appeared in mouse 2 in the 24 hr. sample does not contain *B. subtilis* (verified specifically at the strain level).

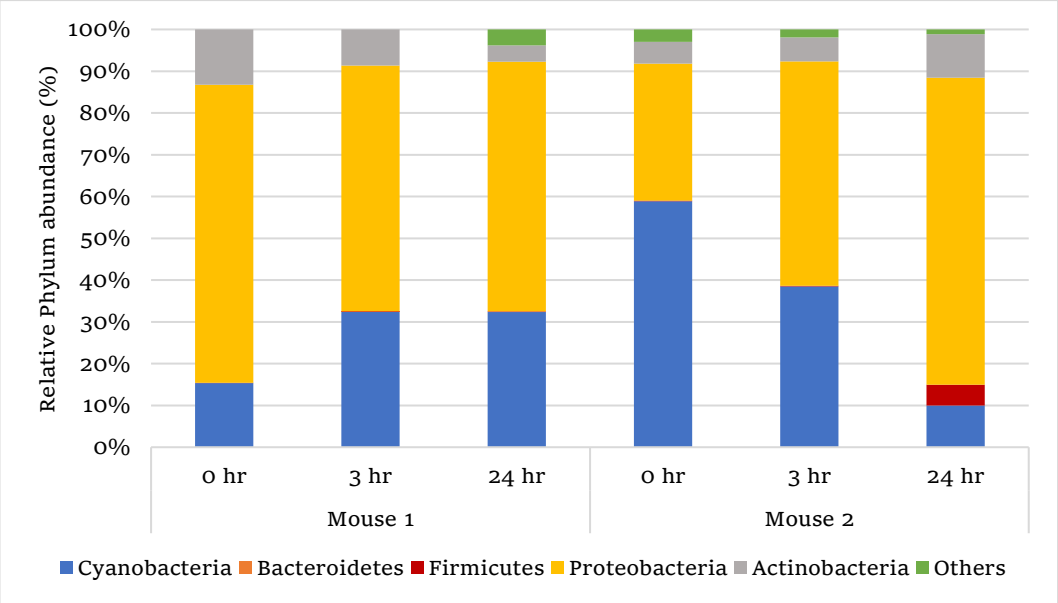

Figure 4.7 *Relative phylum abundance in the native mice skin over time. Two separate biological repeats are presented (mouse 1 and mouse 2).*

In the following step, different mediums were applied on the skin to identify whether they impose any variability to the natural skin microbiome. It can be seen in figure 4.8 that both LB and Pluronic® cause a change in the natural microbiome compositions, right after inoculation and over time. Moreover, in both mediums, a natural variation between the two biological repeats can be observed. In LB, the most significant change in composition can be seen after 24 hours, in both biological repeats. In Pluronic®, both biological repeats present an alteration to the composition of the natural skin microbiome (figure 4.7). The Firmicutes band appeared at 0 hr. at both biological repeats of LB does not contain *B. subtilis* (specifically verified at the strain level).

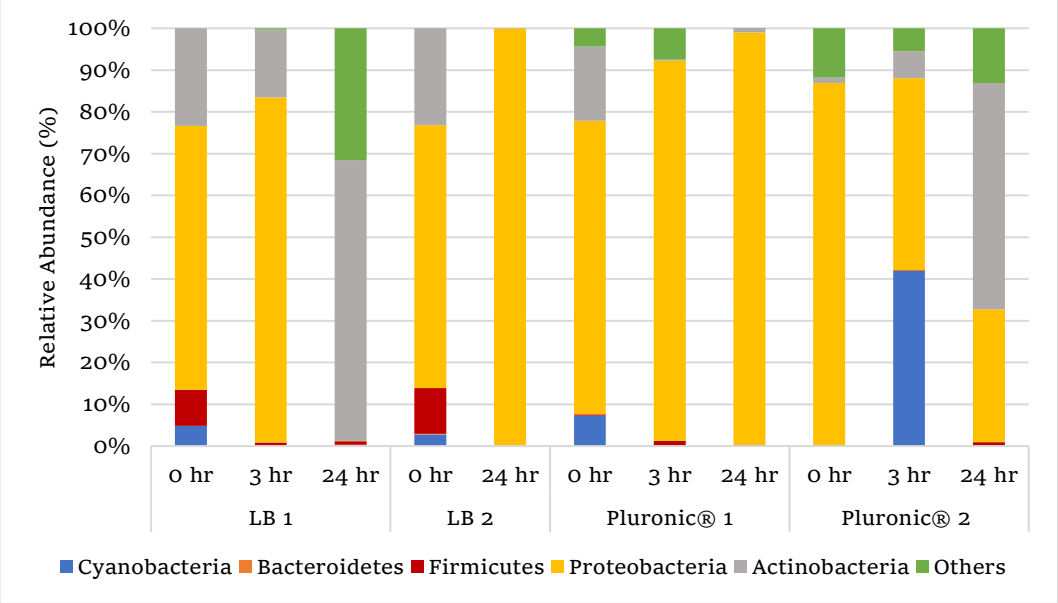

Figure 4.8 *Relative phylum abundance in mice skin with the addition of mediums, over time. Two separate biological repeats are presented for each medium (LB 1 and LB 2, Pluronic® 1 and Pluronic® 2).*

Finally, the skin patches were inoculated with *B. subtilis* in different formulations, as previously explained in section 3.7.2.2. As can be seen in figure 4.9, both biological repeats that contained *B. subtilis* without the pBS3Clux + Pveg plasmid cloned (in LB), show an increase over time in the abundance of Firmicutes (apart from biological repeat no. 2 that shows a decrease after 24 hours). This increase also presented when skin patches were inoculated with *B. subtilis* that was cloned with the pBS3Clux + Pveg plasmid (i.e., an engineered microbiome member) in LB. When the engineered microbiome member was introduced in the Pluronic® polymer instead of LB, biological repeat number 1 showed a slight decrease in Firmicutes abundance after 3 hours. Biological repeat number 2 showed an increase in Firmicutes abundance after 24 hours, which was not as high as the results observed in LB. It was verified in all samples that the firmicutes band represent mostly the strain of *B. subtilis* (i.e., the trends in firmicutes abundance represent the trends in the *B. subtilis* population). These results illustrate and quantify the proliferation of *B. subtilis ex-vivo* (in correlation with the results from the imaging assay performed).

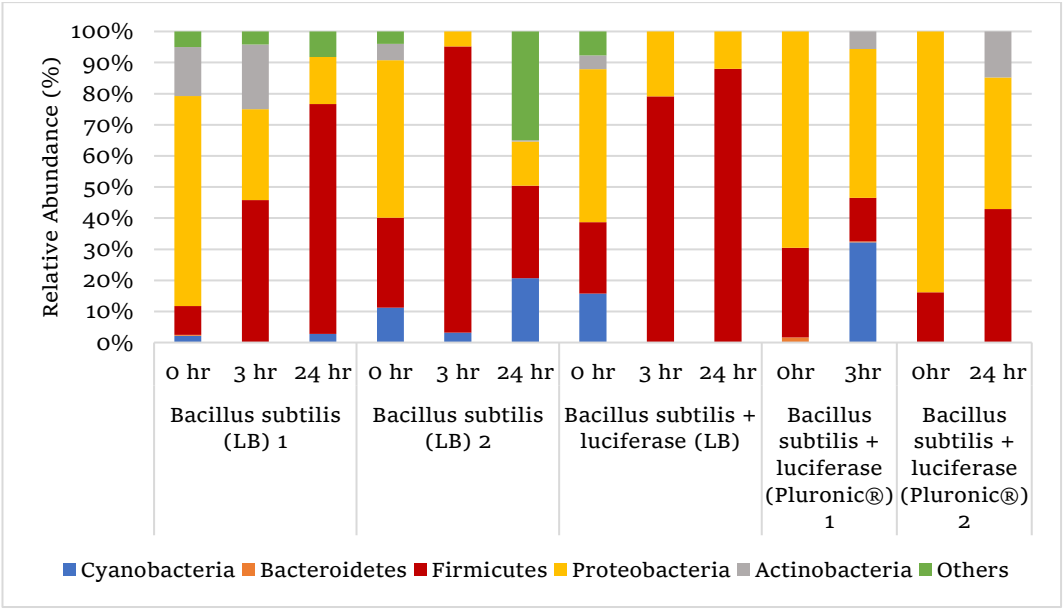

Figure 4.9 *Relative phylum abundance in mice skin inoculated with bacteria in different mediums, over time. Biological repeats are presented for Bacillus Subtilis (LB) and Bacillus subtilis + luciferase (Pluronic®) (1 and 2).*

5 Discussion

This thesis aims to describe a novel approach to specifically investigate the skin microbiome and utilize it as a delivery vehicle of therapeutic agents, to offer a potential solution for a variety of skin conditions. I focused on different approaches and methodologies to specifically target the skin microbiome and utilize some of the unique properties of the skin to optimize both the assays developed and the therapeutic solution that was sought.

5.1 Novel Delivery Method of Therapeutic Agents Utilizing Engineered Skin Microbiome

Initially, as a proof of principle, I chose to work with the gram-positive bacteria *B. subtilis* (a member of the human scalp microbiome) as a model microorganism for the expression and secretion of a therapeutic agent, the enzyme 3α-HSD. This enzyme breaks down the hormone that is believed to be the cause of the skin condition MPHL, 5α-DHT, as explained in the introduction section.

From the results presented in sections 4.1 and 4.2, I conclude that I have successfully engineered *B. subtilis* to express and secrete an active 3α-HSD (heterologous protein) to the supernatant.
As presented in figure 4.2, the lysate of the variant without SP fused to 3α–HSD does not seem to express the enzyme. This result indicates that 3α–HSD is likely not stable inside the cell, and only with secretion and conjugation to a signal peptide does a stable and active enzyme forms.

As presented in figure 4.3, I have demonstrated the ability to specifically quantify 5α-DHT using LC-MS. In the future, this ability might provide a method to perform 3α-HSD activity tests from in-vivo biological samples, measuring directly the substrate degradation rate [44]. This method increases the complexity of the assay, as well as its cost, but might be needed for *in-vivo* testing.

The ability to secrete a 3α-HSD might extend to other therapeutic proteins in the future. One possible example might be secretion of one or several of the anticancer proteins (targeting skin cancer) that are listed in the CancerPPD database of anticancer peptides and proteins [54]. The secretion of these proteins, together with a smart polymeric scaffold, might be tested as a continuous anticancer formulation.

A potential challenge for this approach might be the delivery of the therapeutic agent through the skin in an adequate concentration. Besides using a polymeric scaffold that is aimed to enhance the delivery of the engineered microbiome member back to the skin (i.e., the Pluronic® formulation), a synthetic biology approach might also be implemented in the future to enhance the delivery of the secreted therapeutic agents through the skin. It was shown in the literature that using cell-penetrating peptides might enhance the delivery of proteins to different layers of the skin. Conjugating such a protein (e.g., IMT-P8) to the secreted therapeutic agent might increase the amount of the therapeutic agent delivered through the skin [55].

In the future, a clinical trial that will test the suggested formulation (that includes a secreting *B. subtilis* in a smart polymeric scaffold) might establish its therapeutic effect in humans. These trials will examine the therapeutic effect this formulation might have on MPHL and illustrate some of its key properties *in-vivo* (e.g., delivery through the skin and an adequate pharmaceutical concentration of the secreted protein). To achieve this goal, different strains that secrete the enzyme in different activity levels (as presented in table 4.1), as well as different formulations that will enhance the delivery of both the engineered microbiome member and the therapeutic agent, will be tested.

5.2 Skin Microbiome Research Toolbox

Also in the thesis (section 4.4), I demonstrate the ability to image and sequence engineered microbiome member (i.e., The Skin Microbiome Research Toolbox).

The results of the imaging assay demonstrate an active heterologous protein production of an engineered microbiome member in its native environment *ex-vivo* (section 4.4.1.2). This assay can be further tested *in-vivo*, minimizing the change in physical properties of the skin over time. Also demonstrated is the ability to sample, extract and identify through sequencing the different members comprising the natural skin microbiome, both native an engineered, in the NGS assay (section 4.4.2).

When designing these two assays, I took into consideration the unique characteristics of the skin that need to be implemented for its research. An example of this tailoring is the design of the next generation sequencing assay and in particular the sampling and DNA extraction methods, that took into consideration the relatively low microbial biomass that is found on the skin and its unique physical properties (e.g., relatively low hydration level) [20]. Also, I designed the imaging assay to specifically identify the engineered microbiome member among the diverse natural biota, using the heterologous luciferase it expresses [20].

As a follow up of the imaging assay, it is possible to test a secreted version of luciferase, to verify the heterologous secretion from the bacterial cells. This luciferase should be a protein with a simple structure that will be optimal for secretion from *B. subtilis*.
One option might be the NanoLuc® Luciferase [56]. A significant obstacle that has to be addressed is the need for exogenous substrate supplementation (unlike the *luxABCDE* cassette) [57]. As described in the introduction, one of the main advantages of using the *luxABCDE* cassette is its substrate-independent, real-time emission of a bioluminescent signal. This property allows the direct estimation of the correlation between engineered microbiome proliferation and the

bioluminescent signal emitted. With a substrate-depended luciferase, the local concentration of the substrate mix and its availability *ex-vivo* or *in-vivo* will also play a role and will have to be considered when analyzing the bioluminescent imaging results, both in qualitative and quantitative assays. Moreover, it will be essential to verify that the conclusion previously presented in this discussion regarding secreted proteins (i.e., only with secretion and conjugation to a signal peptide does stable and active 3α-HSD forms) also applies to the secreted luciferase. This future assay needs to identify the secreted bioluminescent signal individually, and not the combination of secreted and non-secreted signal (e.g., a result of a luciferase that hasn't been secreted or been released from the cell through cell lysis).

In figure 4.7, the natural composition of the mice microbiome is presented, as part of the NGS assay. The natural variability between the two biological repeats (i.e., two different mice) is in line with what's been described in the literature: strong individual specificity of microbial community composition [1 3 58]. These results served as a baseline for the analysis of effects of different formulations and bacterial compositions on the relative abundance of the skin microbiome (both engineered and natural), as presented in section 4.4.2.2.

5.3 Growth Media And Formulations Alter The Natural Composition Of The Skin Microbiome

An important result that is presented in figure 4.8 is that different mediums (i.e., LB and the Pluronic® polymer) alter the native composition of the skin microbiome over 24 hours. LB is a rich medium that can give priority to the growth of certain bacterial strains, and hence alter the natural composition of the skin microbiome [59]. In the literature, it was reported that Pluronic® (a surfactant) might affect some bacterial strains (e.g., lower the adhesion of microorganisms) [60]. I believe that these properties of the polymer might affect the natural composition of the skin microbiome. There is a difference in the alteration of the natural composition

between the two mediums, as might be expected from two fundamentally different mediums. This effect also correlates to the results of the imaging assay, presented in figure 4.5 – I saw a slight difference in the growth and heterologous protein expression levels between LB and PBS, in favor of the PBS.

It was demonstrated in the literature that different commercially available soaps and cosmetics might affect different natural properties of the skin (e.g., antimicrobial peptide abundance and skin hydration level) and the composition of the natural microbiome [61] [62]. Some cosmetics tested might even introduce new populations to the skin that may eventually affect it [62]. Unlike the cosmetics and soaps described, the materials and formulations used in my experiments were sterilized before use, to minimize the effect of contamination by an external strain. Nevertheless, I did observe an alteration to the natural microbiome. In the future, I suggest testing several formulations using the assays described in The Microbiome Research Toolbox, to find a formulation that alters the microbiome in the least possible way.

5.4 Engineered Microbiome Proliferation In The Native Environment

The NGS assay not only confirmed and quantified the results observed in the imaging assay (i.e., engineered microbiome proliferation in the native environment over time) but also provided a way to quantify the effect an introduction of a new population might have on the natural microbiome. In figure 4.9 it was shown that not only the *B. subtilis* proliferates on the skin over 24 hours, but also that the addition of *B. subtilis* in LB or Pluronic® alters the composition of the natural microbiome. The advantage and the complementary part that the imaging assay provides is the live status of livelihood and heterologous protein production of the engineered microbiome member, two properties that are not presented with the NGS assay. Together, these two assays provide a bigger picture and allow to investigate the skin microbiome in more diverse ways.

I did not observe any prominent change between inoculation with *B. subtilis* that was engineered with a heterologous plasmid and a non-engineered variant (presented in figure 4.9) – both populations (excluding 24 hr. LB 2) present a substantial increase in abundance over time in relatively the same rate. This result is significant because there is no description or comparison of this kind in the literature to the best of my knowledge.

Another possible use of these results (i.e., the proliferation of the engineered bacteria on the skin) might be to create a live bacterial therapy for the skin, which has been suggested in the literature for wild-type bacteria but had not been developed yet [4]. One such example can be to use the strains that show potential growth as probiotics to supplement deficiencies, similarly to what's been done with probiotics taken orally to supplement the gut microbiome. These strains might also secrete therapeutic proteins to enhance further the therapeutic effect against the deficiency, a concept that was previously shown for the gut [63].

5.5 Future Experiments Using The Microbiome Research Toolbox And Conclusions

In future experiments using The Microbiome Research Toolbox, I suggest considering the following. First, using additional biological repeats may decrease overall variation in the results, present a more precise insight into the trends, and decrease the effect of technical variations. Second, applying *in-vivo* sampling as oppose to *ex-vivo* sampling might reduce the effects of the change in physiological properties of the skin over time (e.g., decrease in the moisture of the skin patches).

In addition, a pharmaceutical inoculation concentration of *B. subtilis* needs to be established as part of the clinical trials described (i.e., establishing a therapeutic effect of the formulation). On the one hand, this concentration will provide an observed therapeutic effect, with an adequate secretion of the active therapeutic agent secreted from

the engineered *B. subtilis* cells (e.g., the 3α-HSD enzyme) over a substantial period (to be established). On the other hand, this initial therapeutic concentration aimed to be low enough to minimize the alteration of the natural skin microbiome over time.

In conclusion, the described creation of an engineered bacteria that proliferate on the scalp and continuously secret a therapeutic agent (e.g., 3α-HSD) might address some of the limitations current solutions poses and provide a novel solution for MPHL and other skin conditions. We applied this approach for a US patent application number 15/471,194. The methodologies used in this thesis may be used to test other potential bacterial strains, the secretion of other therapeutic agents, or both. Moreover, the two assays I describe in The Skin Microbiome Research Toolbox provide an insight into the dynamics between different populations and formulations applied and may be used as a feedback system for the further research of the skin microbiome. These two assays may answer two essential needs illustrated in the literature: visualization techniques of the skin microbiome and gathering data in several timepoints [20].

Bibliography

1. Oh J, Byrd AL, Park M, Kong HH, Segre JA. Temporal Stability of the Human Skin Microbiome. *Cell*. 2016;165(4):854-866. doi:10.1016/j.cell.2016.04.008.

2. Grice EA, Kong HH, Conlan S, et al. Topographical and temporal diversity of the human skin microbiome. *Science*. 2009;324(5931):1190-1192. doi:10.1126/science.1171700.

3. Dorrestein PC, Gallo RL, Knight R. Microbial Skin Inhabitants: Friends Forever. *Cell*. 2016;165(4):771-772. doi:http://dx.doi.org/10.1016/j.cell.2016.04.035.

4. Chen YE, Fischbach MA, Belkaid Y. Skin microbiota – host interactions. *Nat Publ Gr*. 2018;553(7689):427-436. doi:10.1038/nature25177.

5. Ellis JA, Sinclair RD. Male pattern baldness: current treatments, future prospects. *Drug Discov Today*. 2008;13(17-18):791-797. doi:10.1016/j.drudis.2008.05.010.

6. Gonzalez ME, Cantatore-Francis J, Orlow SJ. Androgenetic alopecia in the paediatric population: A retrospective review of 57 patients. *Br J Dermatol*. 2010;163(2):378-385. doi:10.1111/j.1365-2133.2010.09777.x.

7. Adil A, Godwin M. The effectiveness of treatments for androgenetic alopecia: A systematic review and meta-analysis. *J Am Dermatology*. 2017;77(1):136-141.e5. doi:10.1016/j.jaad.2017.02.054.

8. Takayasu S, Adachi K. The conversion of testosterone to 17 -hydroxy-5 -androstan-3-one (dihydrotestosterone) by human hair follicles. *J Clin Endocrinol Metab*. 1972;34(6):1098-1101. doi:10.1210/jcem-34-6-1098.

9. Asada Y, Sonoda T, Ojiro M, et al. 5 α -Reductase Type 2 Is Constitutively Expressed in the Dermal Papilla and Connective Tissue Sheath of the Hair Follicle. *J Clin Endocrinol Metab*. 2001;86(6):1-6. doi:10.1210/jc.86.6.2875.

10. Olsen EA, Hordinsky M, Whiting D, et al. The importance of dual 5α-reductase inhibition in the treatment of male pattern hair loss: Results of a randomized placebo-controlled study of dutasteride versus finasteride. *J Am Acad Dermatol*. 2006;55(6):1014-1023. doi:10.1016/j.jaad.2006.05.007.

11. Kaufman KD, Olsen EA, Whiting D, et al. Finasteride in the treatment of men with androgenetic alopecia. *J Am Acad Dermatol*. 1998;39(4 I):578-589. doi:10.1016/S0190-9622(98)70007-6.

12. Liao A-H, Lu Y-J, Lin Y-C, Chen H-K, Sytwu H-K, Wang C-H. Effectiveness of a Layer-by-Layer Microbubbles-Based Delivery System for Applying Minoxidil to Enhance Hair Growth. *Theranostics*. 2016;6(6):817-827. doi:10.7150/thno.14932.

13. Lin HK, Jez JM, Schlegel BP, Peehl DM, Pachter J a, Penning TM. Expression and characterization of recombinant type 2 3 alpha-hydroxysteroid dehydrogenase (HSD) from human prostate: demonstration of bifunctional 3 alpha/17 beta-HSD activity and cellular distribution. *Mol Endocrinol*. 1997;11(13):1971-1984. doi:10.1210/mend.11.13.0026.

14. Askonas LJ, Ricigliano JW, Penningt TM. The kinetic mechanism catalysed by homogeneous rat liver 3x-hydroxysteroid dehydrogenase. *Biochem J*. 1991;278(3):835-841. doi:10.1042/bj2780835.

15. Wang G, Xia Y, Gu Z, et al. A new potential secretion pathway for recombinant proteins in Bacillus subtilis. *Microb Cell Fact*. 2015;14(1):179. doi:10.1186/s12934-015-0374-6.

16. van Dijl JM, Hecker M. Bacillus subtilis: from soil bacterium to super-secreting cell factory. *Microb Cell Fact*. 2013;12(1):3. doi:10.1186/1475-2859-12-3.

17. Kang Z, Yang S, Du G, Chen J. Molecular engineering of secretory machinery components for high-level secretion of proteins in Bacillus species. *J Ind Microbiol Biotechnol*. 2014;41(11):1599-1607. doi:10.1007/s10295-014-1506-4.

18. Hoffman AS. "Intelligent" Polymers in Medicine and Biotechnology. *Artif Organs*. 1995;19(5):458-467. doi:10.1111/j.1525-1594.1995.tb02359.x.

19. Liu TY, Hu SH, Liu DM, Chen SY, Chen IW. Biomedical nanoparticle carriers with combined thermal and magnetic responses. *Nano Today*. 2009;4(1):52-65. doi:10.1016/j.nantod.2008.10.011.

20. Kong HH, Andersson B, Clavel T, et al. Performing Skin Microbiome Research: A Method to the Madness. *J Invest Dermatol*. 2017;(October):1-8. doi:10.1016/j.jid.2016.10.033.

21. Meighen E. Genetics of bacterial bioluminescence. *Annu Rev Genet*. 1994;28:117-139. doi:10.1146/annurev.genet.28.1.117.

22. La Rosa SL, Diep DB, Nes IF, Brede DA. Construction and application of a luxabcde reporter system for real-time monitoring of enterococcus faecalis gene expression and growth. *Appl Environ Microbiol*. 2012;78(19):7003-7011. doi:10.1128/AEM.02018-12.

23. Anderson S. Shotgun DNA sequencing using cloned DNase I-generated fragments. *Nucleic Acids Res*. 1981;9(13):3015-3027. doi:10.1093/nar/9.13.3015.

24. Nakatsuji T, Chen TH, Butcher AM, et al. A commensal strain of Staphylococcus epidermidis protects against skin neoplasia. *Sci Adv*. 2018;4(2):eaao4502. doi:10.1126/sciadv.aao4502.

25. Allhorn M, Arve S, Brüggemann H, Lood R. A novel enzyme with antioxidant capacity produced by the ubiquitous skin colonizer Propionibacterium acnes. *Sci Rep*. 2016;6(August):36412. doi:10.1038/srep36412.

26. Clontech. Stellar™ Competent Cells Protocol PT5055-2. 2011;6880(0):2.

27. TaKaRa Bio Inc. B . subtilis Secretory Protein Expression System Product Manual. *B.subtilis Secret Protein Expr Syst Prod Man*. 2014;(v201210Da).

28. Kimoto T, Ishii H, Higo S HY and KS. Rattus norvegicus aldo-keto reductase family 1, member C14 (Akr1c14), mRNA. NCBI. https://www.ncbi.nlm.nih.gov/nuccore/NM_138547.3. Published 2010.

29. Radeck J, Kraft K, Bartels J, et al. The Bacillus BioBrick Box: generation and evaluation of essential genetic building blocks for standardized work with Bacillus subtilis. *J Biol Eng*. 2013;7(1):29. doi:10.1186/1754-1611-7-29.

30. IGEM12_LMU-Munich. Part:BBa_K823003. iGEM Registry of Standart Biological Parts. http://parts.igem.org/Part:BBa_K823003.

31. Chen J, Fu G, Gai Y, Zheng P, Zhang D, Wen J. Combinatorial Sec pathway analysis for improved heterologous protein secretion in Bacillus subtilis: identification of bottlenecks by systematic gene overexpression. *Microb Cell Fact*. 2015;14:92. doi:10.1186/s12934-015-0282-9.

32. J H, P R, B K, et al. Use of a Sec signal peptide library from Bacillus subtilis for the optimization of cutinase secretion in Corynebacterium glutamicum. *Microb Cell Fact*. 2016:1-11. doi:10.1186/s12934-016-0604-6.

33. Soerensen DD, Pedersen LJ. Infrared skin temperature measurements for monitoring health in pigs: A review. *Acta Vet Scand*. 2015;57(1). doi:10.1186/s13028-015-0094-2.

34. Olm MR, Brown CT, Brooks B, et al. Identical bacterial populations colonize premature infant gut, skin, & oral microbiomes & exhibit different in situ growth rates. *Genome Res*. 2017;27(4):601-612. doi:10.1101/gr.213256.116.

35. Illumina. 16S Metagenomic Sequencing Library Preparation. *Illumina.com*. 2013;(B):1-28. http://support.illumina.com/content/dam/illumina-support/documents/documentation/chemistry_documentation/16s/16s-metagenomic-library-prep-guide-15044223-b.pdf.

36. Caporaso JG, Kuczynski J, Stombaugh J, et al. QIIME allows analysis of high-throughput community sequencing data. *Nat Methods*. 2010;7(5):335-336. doi:10.1038/nmeth.f.303.

37. Martin M. Cutadapt removes adapter sequences from high-throughput sequencing reads. *EMBnet.journal*. 2011;17(1):10. doi:10.14806/ej.17.1.200.

38. Wilson M. *Microbial Inhabitants of Humans*.; 2004. doi:10.1186/1471-2180-9-259.

39. Kaptan Ölmez H, Aran N. Modeling the growth kinetics of Bacillus cereus as a function of temperature, pH, sodium lactate and sodium chloride concentrations. *Int J Food Microbiol*. 2005;98(2):135-143. doi:10.1016/j.ijfoodmicro.2004.05.018.

40. Saegusa Y, Tabata H. Usefulness of infrared thermometry in determining body temperature in mice. *J Vet Med Sci*. 2003;65(12):1365-1367. doi:10.1292/jvms.65.1365.

41. Stadlbauer V, Leber B, Lemesch S, et al. Lactobacillus casei Shirota supplementation does not restore gut microbiota composition and gut barrier in metabolic syndrome: A randomized pilot study. *PLoS One*. 2015;10(10):1-14. doi:10.1371/journal.pone.0141399.

42. 3-alpha-hydroxysteroid dehydrogenase. uniprot. http://www.uniprot.org/uniprot/P23457. Accessed July, 2016.

43. Western blot troubleshooting tips. *Abcam*. 2016:9-11.

44. Owen LJ, Wu FC, Büttler RM, Keevil BG. A direct assay for the routine measurement of testosterone, androstenedione, dihydrotestosterone and dehydroepiandrosterone by liquid chromatography tandem mass spectrometry. *Ann Clin Biochem*. 2016;53(5):580-587. doi:10.1177/0004563215621096.

45. Ke Y, Bertin J, Gonthier R, Simard JN, Labrie F. A sensitive, simple and robust LC-MS/MS method for the simultaneous quantification of seven androgen- and estrogen-related steroids in postmenopausal serum. *J Steroid Biochem Mol Biol*. 2014;144(PB):523-534. doi:10.1016/j.jsbmb.2014.08.015.

46. 5α-Androstan-17β-ol-3-one. Sigma-Aldrich. https://www.sigmaaldrich.com/catalog/product/sigma/a8380?lang=en&region=IL. Accessed July, 2016.

47. Dulbecco's Phosphate Buffered Saline. Biological Industries USA, Inc. http://www.bioind.com/dpbs-no-calcium-no-magnesium-1218/. Accessed May, 2016.

48. Castelino M, Eyre S, Moat J, et al. Optimisation of methods for bacterial skin microbiome investigation: primer selection and comparison of the 454 versus MiSeq platform. *BMC Microbiol*. 2017;17(1):23. doi:10.1186/s12866-017-0927-4.

49. Metcalf JL, Wegener Parfrey L, Gonzalez A, et al. A microbial clock provides an accurate estimate of the postmortem interval in a mouse model system. *Elife*. 2013;2:e01104. doi:10.7554/eLife.01104.

50. Bouslimani A, Porto C, Rath CM, et al. Molecular cartography of the human skin surface in 3D. *Proc Natl Acad Sci U S A*. 2015;112(17):E2120-9. doi:10.1073/pnas.1424409112.

51. Invitrogen, Scientific T. PureLink ™ Microbiome DNA Purification Kit. 2015;10024(4473979):2-5.

52. Engel P, James RR, Koga R, Kwong WK, McFrederick QS, Moran NA. Standard methods for research on *Apis mellifera* gut symbionts. *J Apic Res*. 2013;52(4):1-24. doi:10.3896/IBRA.1.52.4.07.

53. Belheouane M, Gupta Y, Künzel S, Ibrahim S, Baines JF. Improved detection of gene-microbe interactions in the mouse skin microbiota using high-resolution QTL mapping of 16S rRNA transcripts. *Microbiome*. 2017;5(1):59. doi:10.1186/s40168-017-0275-5.

54. Tyagi A, Tuknait A, Anand P, et al. CancerPPD: A database of anticancer peptides and proteins. *Nucleic Acids Res*. 2015;43(D1):D837-D843. doi:10.1093/nar/gku892.

55. Gautam A, Nanda JS, Samuel JS, et al. Topical Delivery of Protein and Peptide Using Novel Cell Penetrating Peptide IMT-P8. *Sci Rep*. 2016;6:1-13. doi:10.1038/srep26278.

56. Hall MP, Unch J, Binkowski BF, et al. Engineered luciferase reporter from a deep sea shrimp utilizing a novel imidazopyrazinone substrate. *ACS Chem Biol*. 2012;7(11):1848-1857. doi:10.1021/cb3002478.

57. Promega. Nano-Glo® Luciferase Assay System. 2012:19. http://www.promega.com/~/media/Files/Resources/Protocols/Technical Manuals/0/ONE-Glo Luciferase Assay System Protocol.pdf. Accessed December, 2017.

58. Oh J, Byrd AL, Deming C, et al. Biogeography and individuality shape function in the human skin metagenome. *Nature*. 2014;514(7520):59-64. doi:10.1038/nature13786.

59. HiMedia Laboratories. Luria Broth Technical Data M575. 2015.

60. Treter J, Bonatto F, Krug C, Soares GV, Baumvol IJR, Macedo AJ. Washing-resistant surfactant coated surface is able to inhibit pathogenic bacteria adhesion. *Appl Surf Sci*. 2014;303:147-154. doi:10.1016/j.apsusc.2014.02.123.

61. Two AM, Nakatsuji T, Kotol PF, et al. The Cutaneous Microbiome and Aspects of Skin Antimicrobial Defense System Resist Acute Treatment with Topical Skin Cleansers. *J Invest Dermatol*. 2016;136(10):1950-1954. doi:10.1016/j.jid.2016.06.612.

62. Jung H, Sang L, Jeong E, et al. Effects of cosmetics on the skin microbiome of facial cheeks with different hydration levels. 2017;(October):1-14. doi:10.1002/mbo3.557.

63. Ryan PM, Patterson E, Kent RM, et al. Recombinant Incretin-Secreting Microbe Improves Metabolic Dysfunction in High-Fat Diet Fed Rodents. *Sci Rep*. 2017;7(1):1-12. doi:10.1038/s41598-017-14010-x.

המחקר נעשה בהנחיית פרופ' משנה רועי עמית בפקולטה להנדסת ביוטכנולוגיה ומזון.

אני מודה לטכניון על התמיכה הכספית הנדיבה בהשתלמותי.

חקר ושימוש במיקרוביום הטבעי של העור תוך ניצול כלים בביולוגיה סינטטית

חיבור על מחקר

לשם מילוי חלקי של הדרישות לקבלת התואר מגיסטר למדעים בהנדסת ביוטכנולוגיה ומזון

אלכסיי טומסוב

הוגש לסנט הטכניון – מכון טכנולוגי לישראל

אדר ה'תשע"ח חיפה מרץ 2018

חקר ושימוש במיקרוביום הטבעי של העור תוך ניצול כלים בביולוגיה סינטטית

אלכסיי טומסוב

תקציר

בשנים האחרונות, לא פעם הוכחה חשיבותו של המיקרוביום (אוכלוסיות המיקרואורגניזמים שנמצאות על העור) הטבעי שעל העור והשפעותיו על מחלות שונות.
מחלות עור שונות גורמות לשינויים במיקרוביום, אך הקשר בין המיקרוביום למחלות אלו אינו פוענח עד תום. בנוסף, מעט מאוד ידוע על יציבותם של מיקרואורגניזמים השייכים למיקרוביום, שעברו תהליך של הנדסה גנטית ומוחזרים לסביבתם הטבעית. מטרת מחקר זה היא שימוש בכלים מתקדמים ועדכניים בביולוגיה סינטטית לביסוס הפוטנציאל התרפויטי של המיקרוביום המהונדס.

במחקר זה, פיתחתי מספר תבחינים לזיהוי הגורמים הנחוצים לשילוב יציב של חיידק המבטא ומפריש חלבון הטרולוגי בצורה רציפה, אל תוך אוכלוסיית המיקרוביום הטבעית המצויה על העור. במהלך המחקר, הדגמתי את היכולת להפריש חלבון הטרולוגי תרפויטי בחיידק השייך למיקרוביום הטבעי של הקרקפת, בצילוס סבטיליס (בקשת פטנט מספר 15/471,194 שהוגשה בארצות הברית). חלבון תרפויטי זה (3α-HSD) מפרק באופן טבעי את ההורמון שהצטברותו על הקרקפת נחשבת כגורם להתקרחות גברית. על כן, פירוק האנדרוגן על ידי האנזים יכול להוות פתרון להתקרחות הגברית. באמצעות תבחין שפותח, הראתי יכולת להפריש 3α-HSD הפעיל פי 2.3 מאשר בחיידק ללא ביטוי החלבון. בנוסף, הראתי בעזרת תספיג חלבון ספציפי לשייר שצומד לחלבון כי אכן החלבון מצוי בנוזל העליון של החיידק. החיידק המפריש ישולב בתוך מעטפת פולימרית שתגיב לחום הגוף, ותאפשר שחרור מבוקר של החיידק המפריש בצורה מקומית על העור.

בנוסף, פיתחתי שני תבחינים הכוללים מגוון כלים למעקב אחר החיות, ביטוי חלבונים הטרולוגיים ומעקב אחר היחסים הדינאמיים עם אוכלוסיות טבעיות אחרות של החיידק המהונדס שמקורו במיקרוביום הטבעי של העור. הצורך במטרות אלה הובא לא פעם בספרות העכשווית, המדגישה את הצורך בסט כלים אחיד לביצוע מחקר במיקרוביום של העור. שני התבחינים מיועדים להיות משלימים האחד לשני. התבחין הראשון מיועד להדמיה של בצילוס סבטיליס אליו הונדס חלבון שכאשר מבוטא, מפיץ סיגנל ביו-לומינסנטי. סיגנל זה מופץ באופן אוטונומי, ללא צורך בהוספת סובסטרט חיצוני.

בנוסף, זמן מחצית החיים של החלבון קצר מאוד, קרי הופעת אות ביו-לומינסנטי בתבחין תצביע על ביטוי אקטיבי של החלבון בתא. התבחין המתואר נבדק על צלחת פטרי (לאימות שיבוט חיובי), ובנוסף לכך, פוזר החיידק המהונדס על פיסת עור חזיר על מנת לבחון את החיות, השגשוג וביטוי החלבון ההטרוגני אקס ויוו. הגידול המתואר על העור נעשה עם ובלי מצע גידול עשיר, על מנת לבדוק גם את יכולת השגשוג והביטוי בתנאים הטבעיים על העור ללא מצע גידול. מן התוצאות עולה כי החיידק משגשג ומבטא את החלבון ההטרוגני (כאמור, מבוטא כאות ביו-לומינסנטי) הן על צלחת המעבדה, והן בסביבה הטבעית, גם ללא תוספת מצע גידול. ביטוי החלבון על העור נראה גם לאחר 24 שעות.

התבחין השני שפותח ביקש לכמת את השגשוג של החיידק המהונדס והשפעתו, כמו גם השפעות של מצעים ופורמולציות, על המיקרוביום הטבעי של העור. הכימות נעשה בעזרת שיטת ריצוף מהדור החדש – רוצף מקטע V1-V3 של הגן לחומצה ריבונוקלאית ריבוזומית. פיסות עור עכבר אולחו במגוון פורמולציות, ודנ"א (חומצה דאוקסיריבונוקלאית) הופק לצרכי ריצוף במספר נקודות זמן (0, 3 ו 24 שעות). מתוצאות תבחין זה עולה כי המיקרוביום הטבעי נשאר זהה בעבור אותם פרטים אז שונה בין פרטים. בנוסף, תוספת מצעים כגון מצע LB והפורמולציה הפולימרית שתוארה (ללא חיידקים) משנה את הרכב המיקרוביום לאורך זמן. כאשר הוסף החיידק (עם ובלי פלסמיד הטרוגני), נצפתה עליה משמעותית באחוז החיידק לאורך זמן, תוך שינוי הרכב המיקרוביום (בLB). לעומת זאת, כאשר הוסף החיידק בתוך פורמולציה פולימרית, לא נצפתה עליה חדה כמו בLB – יתכן ומתן החיידק בפורמולציה תהיה עדיפה ותשנה פחות את הרכב המיקרוביום.